Enhancing Carbon based Supercapacitor performance through Redox additive based Gel Polymer Electrolyte

A thesis submitted towards partial

fulfilment of the requirements for the degree of

Master of Technology in

Nano Science and Technology

Submitted by

Kingshuk Chakraborty

Roll No: 002230701002

Exam Roll No: M4NST24002

Registration No.: 163807 of 2022-2023

Under the guidance of

Prof. (Dr.) Kalyan Kumar Chattopadhyay

Department of Physics &

School of Materials Science and Nanotechnology

Jadavpur University

Jadavpur University

Kolkata-700032

India

2024

CERTIFICATE OF RECOMMENDATION

This is to clarify that the thesis entitled **"Enhancing Carbon based Supercapacitor performance through Redox additive based Gel Polymer Electrolyte''** is a bonafide work carried out by KINGSHUK CHAKRABORTY under our supervision and guidance for partial fulfilment of the requirement of Master of Technology (Nano Science and Technology) in School of Materials Science and Nano Technology, during the academic session 2022-2024.

SUPERVISOR
Prof. (Dr.) Kalyan Kumar Chattopadhyay
Department of Physics
Jadavpur University, Kolkata-700032

DIRECTOR
Dr. Mahua Ghosh Chaudhuri
School of Materials Science and Nanotechnology Jadavpur University, Kolkata-700032

DEAN
Faculty Council of Interdisciplinary Studies,
Law and Management (FISLM)
Jadavpur University, Kolkata-700032

CERTIFICATE OF APPROVAL

This forgoing thesis is hereby approved as a credible study of an engineering subject carried out and presented in a manner satisfactorily to warranty its acceptance as a prerequisite to the degree for which it has been submitted. It is understood that by this approval the undersigned do not endorse or approve any statement made or opinion expressed or conclusion drawn therein but approve the thesis only for purpose for which it has been submitted.

Committee of final examination for evaluation of thesis

** Only in case the thesis is approved.

Acknowledgement

In the first place, I would like to express my profound gratitude to my supervisor **Prof (Dr). Kalyan Kumar Chattopadhyay** for his advice and guidance from the very early stage of this research as well as giving me extraordinary experiences throughout the work. Above all and the most needed, he provided me constant encouragement and support in various ways. Thankyou also for the amicable environment conducive to extensive research work at Thin Film and Nanoscience Lab, in which you have welcomed me. All these provided me great support, helping me to confront the difficult periods of my project, which I do not think I would have completed it otherwise.

I want to extend my gratitude to my co-supervisor **Dr. Pulak Pal** (Assistant Professor, Department of Physics Raja Peary Mohan College, Uttarpara, West-Bengal, India) for his advices, guidance, and crucial contribution throughout my work. His involvement with his originality has triggered and nurtured my scholarly development that I will benefit from, for along time to come. I really cannot value his support and generous cooperation. He has been like an elder brother to me always by my side whenever needed him.

I would also like to express my sincere thanks to Prof. Sourav Sarkar, Prof. C.K. Ghosh, Dr. Mahua Ghosh Chowdhury for their help, support, encouragement, suggestion and advice during the course of the research. Their enthusiasm provided me a helpful and effective way of learning which in turn inspired me to follow the research project with great enthusiasm.

I would also really like to thank all the staff members of School of Materials Science and Nanotechnology and Department of Physics for carrying out the critical characterization parts of the synthesized samples that composed a very important part of the thesis.

I extend my heartiest thanks to all my seniors of 'Thin Film & Nano Science' lab especially, Shuvankar Podder da, Abhirup da, Sreya di, Pulak da, Nabanita di, Nabamita di, Ratna di, and everyone in this lab for extending their helping hands. I would also like to thank all my friends Aritra, Ankita, Prasenjit, Soumili, Koustav, Arnab, Arijit, Amrita Sourav and all of them for their encouragement and cooperation.

Finally, I express my special gratitude to my parents and all my well-wishers for their wholehearted support, love and encouragement.

Abstract

The work described in the thesis has been done with a motive to synthesize gel polymer electrolytes which act as **self-separators** and their application in the fabrication of EDLC based supercapacitor. The use of plasticizers and Ionic Liquids is described in the literature review and the synthesis process describes how the redox additive based supercapacitor are synthesized. The Gel Polymer Electrolyte (GPE) based EDLC devices fabricated with standard activated carbo electrodes show a significant enhancement of specific capacitance of the supercapacitor fabricated. We have used the measurements from Cyclic Voltammetry (CV) Galvanostatic Charge Discharge (GCD) and Electrochemical Impedance Spectroscopy (EIS) to reach an optimization of the specific capacitance value. The different weight percentage of redox additives that we have used gave us a promising result. The physiochemical properties of the electrolyte is studied such as cation size and their effects on the electrochemical performance thus we try to establish a co-relation between the electrochemical performance of EDLC and the physiochemical property of Ionic Liquid. We obtain the values of Specific Capacitance from Galvanostatic Charge Discharge Method as 126 F g^{-1} for GPE with CsI additive and 87.8 F g^{-1} for GPE having no redox additive showcasing an enhancement. Its Power and Energy density were also calculated

Contents:

Chapter 1: Introduction and Objective…….1-27

Chapter 2: Literature Review……28-36

Chapter 3: Sample Preparation…….37-45

Chapter 4: Instruments and Apparatus…….46-68

Chapter 5: Characterization of Gel Polymer Electrolytes (GPE) and Results…….69-88

Chapter 6: Conclusion and Scope of Future Work…….89-96

Chapter 1:

Introduction and Objective

1.1 Nanostructures and nanotechnology

The study of extremely small objects and their usage in various scientific disciplines, including biology, physics, chemistry, and materials science, are the subjects of nanoscience and nanotechnology. The word 'Nano' means one billionth of a meter" (From the talk **There's Plenty of Room at the Bottom**, delivered by Richard P. Feynman at the annual meeting of the American Physical Society).

The concept of nanotechnology was coined for the first time by the eminent physicist Richard Feynman in 1959 in his lecture which was published in 1960 enfranchised 'There's Plenty of Room at the Bottom' [1]. The term 'nano-technology' was first used by Norio Taniguchi in 1974 although it is not very well known to people since centuries. In 1986 inspired by Feynman's concept, K. Eric Drexler used the word 'nanotechnology' in book 'Engines of Creation: The Coming Era of Nanotechnology [2].

Nanoscience is the study of objects that typically range in size from 1 to 100 nm in at least one direction. It is possible to change the mechanical, electric, optical, and magnetic properties of matter if it is broken up into such tiny units [3]. Bulk properties would diminish and nano properties would dominate. Quantum effects due to the size limitation come into play. Nanoscience and Nanotechnology are interdisciplinary topic, crossing the boundaries between physics, chemistry, chemical, electrical, mechanical, and electronics engineering. One of the most significant developments in the previous several decades is thought to be nanoscience. Several basic Newtonian principles do not apply at the nanoscale, necessitating the development of new technologies. A symbiotic link exists between nanoscience and technology. New technological developments follow scientific discoveries, which then lead to implementations. Two new technologies which enabled the progress of nanoscience are scanning tunnelling (STM) and scanning force microscopy (SFM). They allow to image of structure and manipulate objects on surfaces with enough precision even in ambient conditions or in liquids.

Any technology with applications in the real world that operates on a nanoscale is referred to as nanotechnology. The field of nanotechnology includes the development and applications of physical, chemical, and biological systems at length scales ranging from a single atom or molecule to submicron dimensions, as well as the incorporation of the resulting nanostructure

into larger systems. In the early twenty-first century, nanotechnology is anticipated to have an enormous impact on our economy and society, comparable to that of semiconductor technology, computer technology, or molecular biology. Nanotechnology science and technology research promises innovations in a variety of fields, including materials and manufacturing, nanoelectronics, healthcare, medicine, energy, biotechnology, information technology, and national security. Nanotechnology is thought to be the next Industrial Revolution. Due to the development of novel synthesis pathways and characterization strategies, nanoscience and nanotechnology have rapidly advanced during the last few decades. Nanoscale structures come in many different forms, such as nanotubes, nanowires, and nanosheets. Since they are zero dimensional structures; nanoparticles are also frequently referred to as quantum dots. It is nothing but basic physics acting behind the novel properties of the above systems and it has been well explained by quantum mechanical point of view. In order to understand these systems, it is very essential to discuss the density of states (DOS) of quantum dots (0 dimension), quantum wires (1 dimension) and quantum wells (2 dimensions) in brief. The available electron states in a system can be calculated by the well-known Schrödinger equation: $H_\psi = E_\psi$. Solving this we can finally get the density of states in k-space/ volume. In generalized form,

$$g(E)dE \approx E^2$$

The energy is calculated from the top of the valence band for holes and the bottom of the conduction band for electrons in this case, where d is the degree of dimension. g(E) is a uniform square-root function of energy in the three-dimensional system. Since g(E) in a 2D system is constant, it differs significantly from a 3-D system. Although the density of states in a 2-D system is step-function rather than quasi-continuous, the energy spectrum is [10]. The dependence of DOS on energy changes by $E^{-1/2}$ each time we transition to a lower dimensionality system.

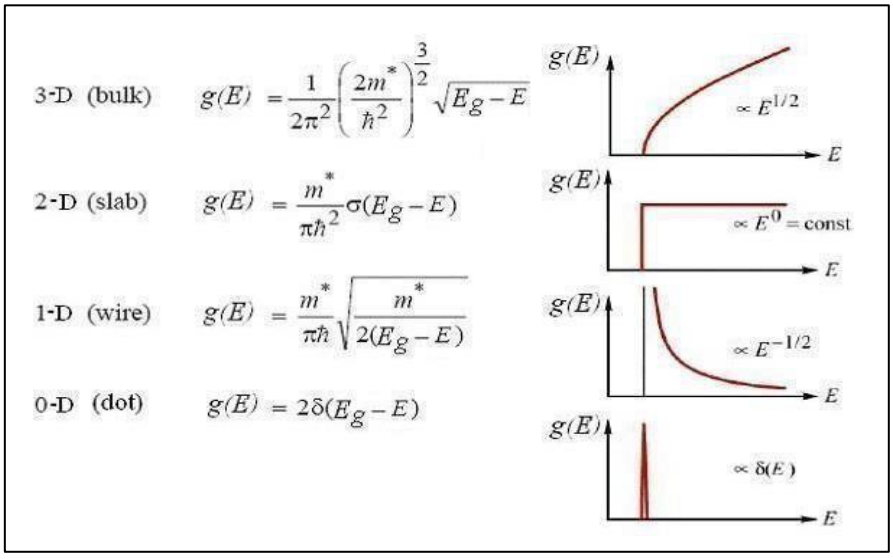


Fig1.1.- Schematic illustration of structural dimensionality of materials with density of states.

Now a quick discussion of the "quantum size effect" is necessary. To achieve this, materials' electrical characteristics are altered while their particle sizes are noticeably reduced. If the reduction in dimension is restricted from macro to micro, this effect has no bearing. On the other hand, the quantum effect becomes quite noticeable at the nanoscale. The electrical structure of nanocrystals is altered by the quantum confinement effect when the diameters of the nanoparticles are equivalent to the Bohr excitonic radius (rB) of those materials. If particle radius (r) in the nanocrystalline materials are less than Bohr radius (r <rB**),** strong quantum confinement effects take place. Weak quantum confinement effects are found within particles having radius larger than Bohr radius (r >r_B**).**

$$\mathbf{E_2 - E_1 = \Delta E = \hbar^2 \pi^2 (n_2^2 - n_1^2) / 2mL^2}$$

The ability of solids to conduct current can vary greatly, and this can be shown by comparing the resistivity of good conductors and insulators. At 1K temperature, the electrical resistivity of pure metal is 10^{-12} ohm–cm. A good insulator has a resistance as high as 10^{22} ohm-cm and can range as wide as 10^{32} ohm-cm. Understanding this astounding range is made possible by the presence of electron band energy in materials [4].

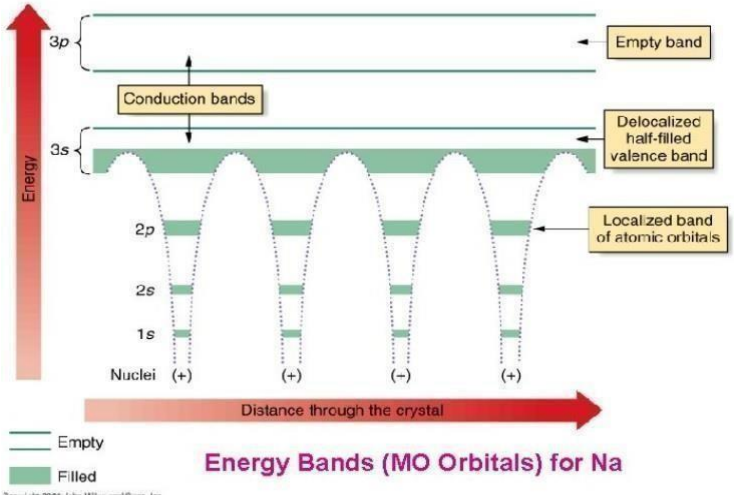


Fig.1.2 The band theory of solids

Above picture shows the band theory of solids. It is seen that the energy bands are formed from the overlap of atomic orbitals of similar energy from all atoms in solids. Energy bands having core electrons (non-valance) are localized and energy bands having valance electrons are delocalized. If we solve the time independent Schrodinger equation, we get, change in energy level.

n = 1,2, 3,…, m = mass of the particle, L = dimension of particle, ħ = Plank's constant

From this equation, we may infer a few things, including the fact that the square of the particle's diameter is inversely related to the shift in energy levels from one state to another. 1. This indicates that the energy difference between two levels rises as we travel from the bulk to the nano size. 2. Different energy levels of minuscule particles are observed to be "quantized." 3. In addition, when the system's mass diminishes, the energy level rises.

Regardless of temperature, metals have a band that is alternately full and empty. They are hence very conductible. By analogy with the valence electrons of individual atoms, the lowest, nearly

entirely occupied band in an insulator or semiconductor is referred to as the valence band. Since current in these materials may only flow when electrons are stimulated to the conduction band, the highest, virtually empty band is known as the conduction band. The only distinction between insulators and semiconductors is the size of the prohibited band gap in the case of insulators, which results in fewer electrons being present there and reduced electrical conductivity. The conductivity of semiconductors is highly influenced by the material's temperature since thermal energy is one of the primary processes by which electrons are driven to the conduction band. Coons has examined the Fermi energy notion in his term project [5].

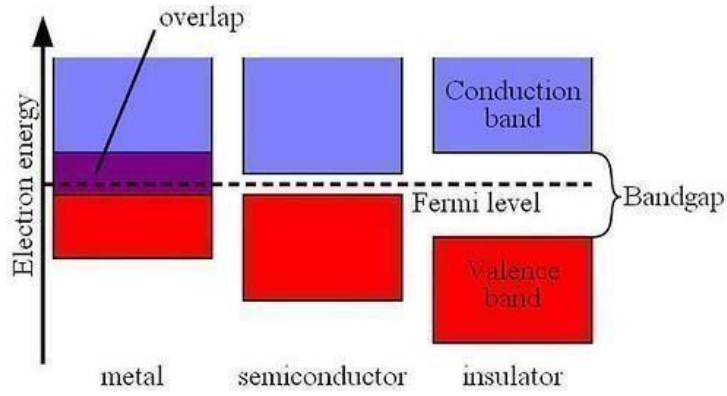


Fig.1.3- Simplified diagram of the electronic band structure of metals, semiconductors, and insulators.

This band gap is one of the most useful aspects of the band structure, as it strongly influences the electrical and optical properties of the material. Electrons can transfer from one band to the other by means of carrier generation and recombination processes. The band gap and defect states created in the band gap by doping can be used to create semiconductor devices such as solar cells, diodes, transistors, laser diodes, and others [6].

1.2 Brief Introduction to Electrochemical Energy Storage/Conversion Device:

The research and development of energy storage/conversion devices field is mainly due

increasing demand of portable and green energy source. There are some basic differences in energy storage and energy conversion device. For energy storage devices reactants are sealed in the container and for energy conversion devices oxidant and reductant are fed into the electrochemical cell so that a permanent flow of electricity can be achieved [6]. The rechargeable lithium-ion batteries and supercapacitors are the example of energy storage devices and fuel cells are the example of energy conversion device [6]. It is needed to study the mapping of power density as a function of energy density (Ragone plot) to gain the wide perspective of these devices which is shown in *Fig. 1.1* [6-7]. It is observed from Ragone plot that the electrochemical double layer (EDL) supercapacitors and fuel cells are situated at two extreme ends on the plot. User can achieve very high output current at very short time period by using electrochemical double layer supercapacitors. Similarly, fuel cells show very high energy density but at the same time exhibit very low power density, indicating that user can draw energy for a longer time period. But if high energy is required in very short time period, fuel cells will not be able to deliver the required energy effectively [8]. On the other hand, the rechargeable batteries are situated at the middle of these two extreme limiting end points which can deliver moderately both high energy and power density. A concise discussion on the structural and working principle of these devices are required for a better understanding of their functionality and also for understanding of the significance of polymer electrolytes in these devices.

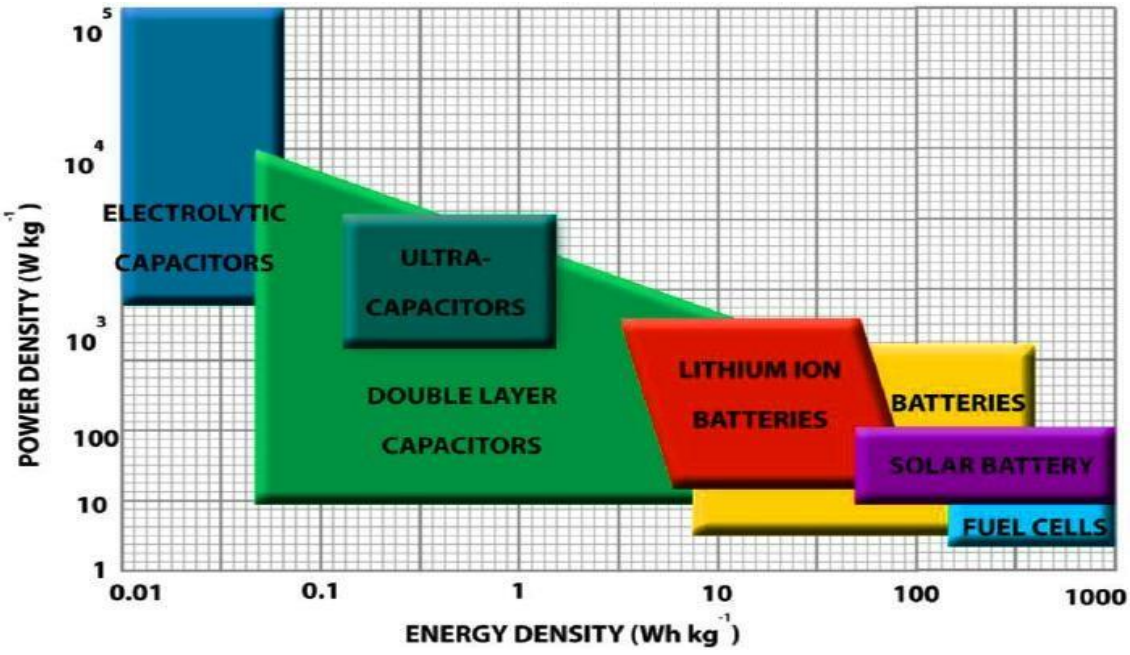


Fig. 1.4 Ragone plot representing a comparative study of energy density and power density of different electrochemical energy storage/conversion devices [6-7].

Supercapacitors

Supercapacitors (SCs), also called electric double-layer capacitors, ultracapacitors or electrochemical capacitors, are emerging as an important class of energy storage devices with very high energy density and a low internal resistance, that are able to store and deliver energy at relatively high speed compared to batteries due to the energy storage mechanism which involves a simple charge separation process at the electrode-electrolyte interface.

Conventional capacitor and supercapacitor and Mechanism

Fig. 1.5 shows the schematic diagram of (a) a conventional capacitor and (b) a supercapacitor. The conventional capacitor has two conducting electrodes and an insulating dielectric material called a separator incorporated to prevent short-circuit between them. When a potential is applied between the two electrodes opposite charges accumulate on the surface of each electrode. The charges can be kept separated by the dielectric material and in this way a conventional capacitor can stores energy [13].

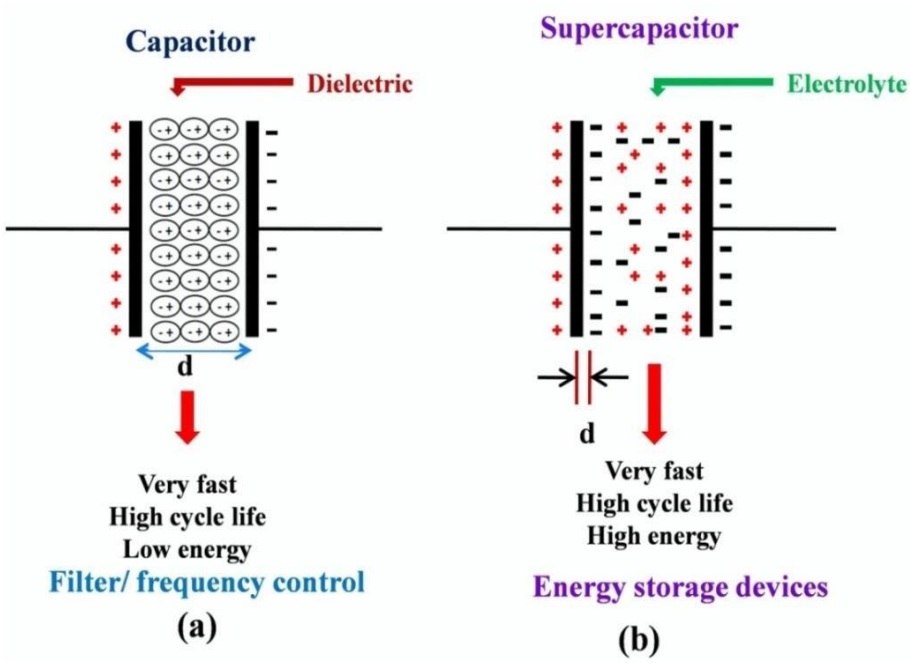


Fig. 1.5 Schematic diagram of (a) a conventional capacitor and (b) a supercapacitor.

The formula of Capacitance is given as:

$$C = \frac{A * \varepsilon_r * \varepsilon_0}{d}$$

where ε_o and ε_r are the dielectric constant of free space and dielectric constant of the insulating material respectively. A and d are the surface area of the each electrode and distance between the electrode respectively. Basically, working principle of capacitor and supercapacitor are very similar. Supercapacitor consists of two conducting electrodes immersed in an electrolyte solution with one separator between them and two current collectors. The difference between plane capacitor and supercapacitor is that electrodes for supercapacitors generally have much higher surface areas than those for plane capacitors and an electrolyte solution in a separator between electrodes. Thus, the capacitance and energy enhances dramatically over that of the plane capacitors due to the higher surface area A and smaller distance d between two electrodes. When charged, the negative ions in the electrolytes will diffuse to the positive electrode, while the positive ions will diffuse to the negative electrodes and creates two separate layers of capacitive storage which form a series circuit of two individual capacitors having capacitances C_1 and C_2. The total capacitance C_{total} is given by

$$C_{total} = \frac{C_1 * C_2}{C_1 + C_2}$$

Supercapacitors may have either symmetric or asymmetric electrodes. For symmetric electrode, values of capacitances are same and total capacitance is half value of each single electrode (if $C_1 = C_2$ then $C_{total} = ½\ C_1$). For asymmetric capacitor, the total capacitance can be taken as that of the electrode with smaller capacitance (if $C_1 >> C_2$ then $C_{total} \approx C_2$).

Classification of supercapacitors

Generally, supercapacitors are classified into main three different classes depending on their working mechanism: (i) electrochemical double-layer capacitors (EDLCs), (ii) pseudo-capacitors, and (iii) hybrid capacitors which are shown in *Fig. 1.5*. All supercapacitors can be characterized by a unique working principle for charge storage which is electrostatic interaction, reversible faradic redox and a combination of the two. The EDLCs store charge through electrostatic interaction between electrode material and charge carriers of electrolyte in which the charge carriers are kept

separately at the electrode-electrolyte interface by physical process. Different carbon-based materials and their derivatives such as activated carbon, carbon nano-tubes, carbon aerogels, graphene, etc. are used as electrode materials for EDLCs [14-16].

Among different carbon materials, porous activated carbons (ACs) have received great attention due to its high specific surface area, good adsorption properties and low cost. For pseudo capacitors, the energy is stored charge by reversible Faradic redox reactions at the surface of the active material which consists of oxidation-reduction reactions. Transition metal oxides such RuO_2, MnO_2, V_2O_5, Fe_3O_4 and α-$Co(OH)_2$, heteroatoms containing covalent organic frameworks and conducting polymers have been used as pseudo capacitor electrode materials to store charge due to their high electrical conductivity and large surface area [17-18]. The third one is hybrid capacitor; the charge storage mechanism is a combination of electrostatic interaction (non-Faradic) and Faradic. The carbon and metal oxide based composite material is used as an electrode material. The electrode materials of all classes of supercapacitor are summarized in *Fig. 1.5*.

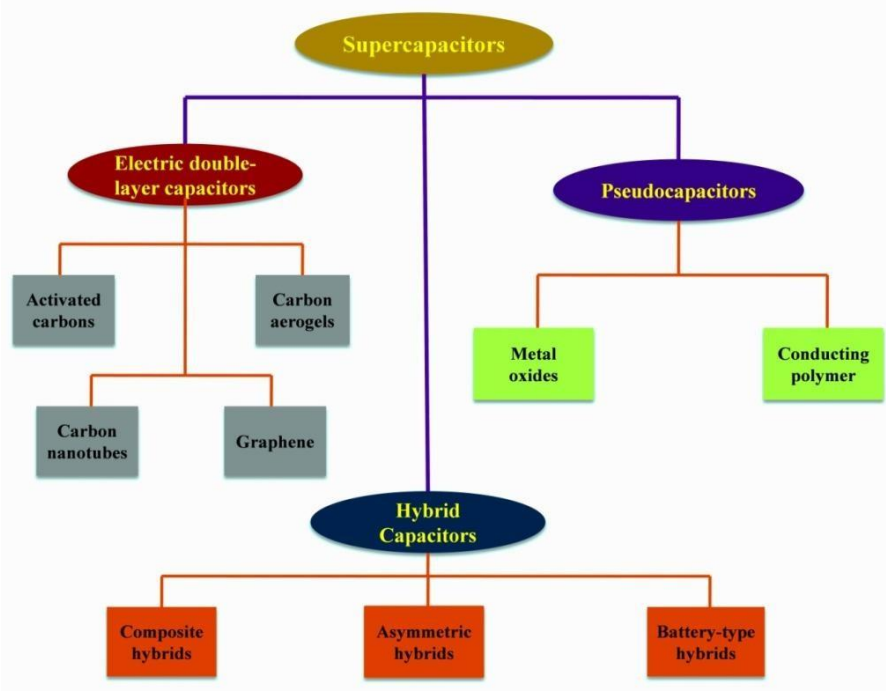


Fig. 1.6 Taxonomy of supercapacitors and their electrode materials

In supercapacitor, an electrically insulating charge carrier-permeable membrane is placed between two electrodes filled with a liquid electrolyte because liquid electrolyte shows high ionic conductivity. As the leakage and corrosion of liquid electrolytes are a matter of

concern, efforts are made to change these liquid electrolytes by using solid/gel electrolytes.These next generation supercapacitors are safe and also provide high performance, bear less weight and can take flexible form. The polymer electrolytes are ideal candidates for flexible solid-state supercapacitors among solid electrolytes.

Fuel Cell

A fuel cell is an electrochemical apparatus that directly converts the chemical energy stored in fuels like hydrogen into electrical energy. Unlike batteries, fuel cells don't require periodic recharging; they continuously produce electricity as long as there's a fuel supply. There are five main types of fuel cells categorized by the polymer electrolyte they utilize: (i) polymer electrolyte membrane (PEM) fuel cells or PEFCs, (ii) solid oxide fuel cells (SOFCs), (iii) alkaline fuel cells (AFCs), (iv) phosphoric acid fuel cells (PAFCs), and (v) molten carbonate fuel cells (MCFCs). Among these, the polymer electrolyte fuel cell (PEFC) is particularly promising due to its operational efficiency.

A PEM fuel cell consists of a proton-conducting polymer electrolyte membrane, an anode, and a cathode. This setup allows for the efficient conversion of chemical energy into electrical energy. Figure 1.6 illustrates the schematic diagram of a PEM fuel cell [19].

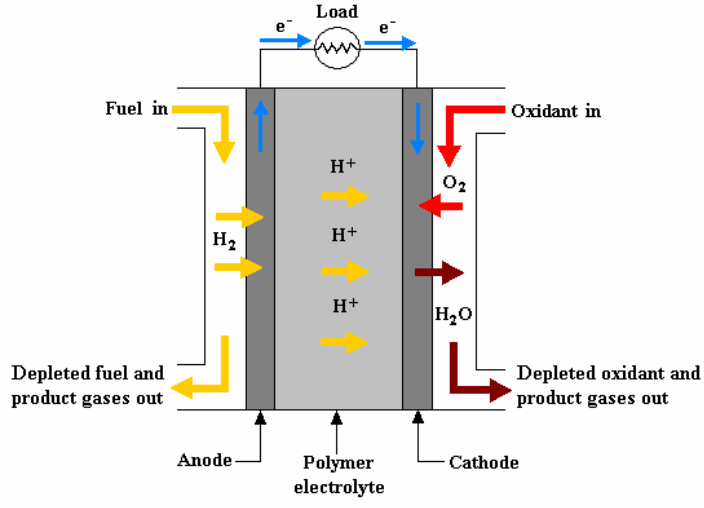


Fig. 1.7 Schematic Diagram of a PEM fuel cell

In a PEM fuel cell, hydrogen flows through the anode while oxygen flows through the cathode. At the anode, hydrogen molecules split into protons and electrons. Protons travel through the polymer electrolyte membrane, while electrons create an electric current in an external circuit, also producing excess heat. At the cathode, protons, electrons, and oxygen

combine to form water molecules. PEFCs can function within a temperature range of 80°C to 100°C, utilizing air or oxygen as the oxidizer and hydrogen as the fuel, achieving up to 60% efficiency in converting electrical energy [20]. To ensure high performance in PEFCs, the proton-conducting polymer electrolyte membranes must meet specific criteria: they should be made of cost-effective materials, exhibit high proton conductivities, possess good water uptake capabilities above 100°C, and demonstrate durability [21].

Ionic Conductors: Brief Overview

Ionic conductors are solid materials with the ability to conduct electricity, characterized by high ionic conductivity (ranging from 10-6 to 10-1 S cm-1) and negligible electronic conductivity (typically 10-9 Scm-1 or lower). The high value of ionic conductivity implies that ions serve as the primary charge carriers, resulting in nearly unity ionic transference numbers. These materials exhibit very low activation energies, typically less than 0.5 eV. Ionic conductors can be categorized in various ways based on factors such as types of charge carriers, conductivity magnitude, microstructure, synthesis methods, and physical properties.

1. Amorphous Ion Conducting Materials: These materials, often referred to as glassy ionic conductors, are prepared using techniques like melt quenching with high quenching rates, sol-gel methods, thermal evaporation, sputtering, and glow-discharge decomposition. They offer advantages such as high isotropic ion conduction with low activation energy at ambient conditions, ease of fabrication into thin films, wide compositional variability, high thermal stability, low electronic conductivity, and absence of grain boundaries. They can be further categorized into cation-conducting (e.g., Ag+, Li+, Na+, Cu+) sulphide/oxide and selenide glasses, as well as anion-conducting glasses.
2. Framework Crystalline/Polycrystalline Ionic Conductors: These materials involve charge carriers migrating within a rigid crystalline framework. Charge carrier migration occurs via both cations and anions. They are prepared through solid-state reactions involving more than one ionic salt, resulting in materials with two sub-lattices: a skeleton and a molten sub-lattice facilitating ion migration. They are divided into soft-framework crystals (SFCs)

   and hard-framework crystals (HFCs). SFCs, being ionic in nature, contain conducting ions with heavy polarizability and exhibit order-disorder phase

transitions and low Debye temperatures. HFCs, on the other hand, are covalent in nature, with conducting ions of low polarizability, relatively high Debye temperatures, and no phase transitions.

3. Gel Electrolytes: These substances contain a solid phase network swollen by a continuous dispersion of a liquid phase, exhibiting properties intermediate between solids and liquids. Gel electrolytes exhibit liquid-like behaviour at both high and low temperatures, making them attractive due to ease of preparation, good thermal properties, high room temperature conductivity, and electrochemical stability. They are typically created using alkaline salts and find applications in various fields including solar cells.
4. Composite Electrolytes/Dispersed Solid Electrolytes: These are solid multiphase systems containing two or more materials mixed to achieve high ionic conductivity at room temperature. They involve dispersing chemically inert and insulating sub-micrometer particles (second phase dispersoids) into a conducting solid host matrix (first phase host matrix). The properties of these materials depend on factors such as dispersoid size, nature, particle size, and preparation method. They can be broadly categorized into crystal-crystal, crystal-glass, glass-polymer, and crystal-polymer composites.
5. Polymer Electrolytes: This class encompasses ionically conducting and electronically insulating solid-phase materials formed when an alkali salt (e.g., LiI, LiBF4, LiClO4, LiTf, LiTFSI) is dissolved into an ion-coordinating polymer. This process, known as complexation, results in polymer electrolytes. They are typically prepared using techniques like standard solution cast, sol-gel, and electro-deposition methods. Conventional polymer salt complexes should ideally be free from additives or contaminants with low molecular weight.

Polymer Electrolytes

Polymer electrolytes, particularly those conducting lithium ions, are pivotal components in various electrochemical devices like rechargeable lithium-ion batteries and supercapacitors, as highlighted earlier. While liquid electrolytes offer high conductivity and interface compatibility with electrode materials, they suffer from leakage and low energy density. Crystalline superionic conductors and glass electrolytes, although highly conductive, are rigid and prone to interface issues with cycling electrodes due to volume changes. In contrast, polymer electrolytes, being flexible, can accommodate such volume changes. The

fundamental electrochemical properties of polymer electrolytes were discussed earlier. In terms of structure and composition, polymer electrolytes can be categorized as follows:

1. Polymer Salt Complexes: These electrolytes involve dissolving alkali metal salts with low dissociation energy into a high molecular weight polymer matrix. The room temperature ionic conductivity of such complexes is typically low, ranging from 10-9 to 10-6 S cm-1.
2. Plasticized Polymer Electrolytes: This type of electrolyte incorporates organic carbonates, glycol-based liquids, or ionic liquids into conventional polymer salt complexes. Ionic liquids, which are salts in liquid state, act as plasticizers and additional sources of charge carriers for electrical conduction.
3. Nano-composite Polymer Electrolytes: Nano-particles with high surface area are added to conventional polymer salt complexes to enhance mechanical stability, ionic conductivity, and electrochemical stability.
4. Polyelectrolyte Membranes: These polymers possess charged functional groups covalently bound to the polymer backbone. They release negative or positive ions when dissolved in a suitable solvent, with the polymer backbone also being charged. Negatively charged backbone-based electrolytes are preferred for many applications.
5. Gel Polymer Electrolytes: These electrolytes consist of liquid electrolytes trapped within a neutral polymer matrix. They exhibit solid-like properties on a macroscopic scale and liquid-like properties on a microscopic scale.

Among these types, gel polymer electrolytes and plasticized polymer electrolytes demonstrate excellent room temperature ionic conductivity (around 10-3 S cm-1) but with reduced mechanical stability. Conversely, polymer salt complexes, nano-composite electrolytes, and polyelectrolyte membranes offer good mechanical stability with moderate ionic conductivity (around 10-5 S cm^{-1}).

Characteristics of Different Host Polymer Matrix

A polymer matrix is a large molecule made up of repeated identical subunits, known as monomers, linked together by covalent bonds. The structure of polymers can vary, with differences arising from whether they have a 1-D, 2-D, or 3-D structure, based on how the atoms and chains are connected in space. The properties of polymer matrices are influenced

by factors such as chemical composition, molecular weight, and morphology.

For a polymer matrix to serve effectively as a host for electrolytes, it should possess certain characteristics:

- The atoms or groups of atoms within the polymer matrix should have enough electron-donating power to form coordinate bonds with cations.

- The polymer matrix should have a high molecular weight and a low crystalline phase.
- There should be low barriers to bond rotation, allowing for easy segmental motion of the polymer chains.
- There should be an appropriate distance between the coordinating centers to facilitate efficient ion transport.

Poly(vinylidene-fluoride-hexafluoropropylene), P(VdF-HFP):

P(VdF-HFP) is a copolymer that has recently garnered attention for its use in polymer electrolytes. It consists of both crystalline poly(vinylidene fluoride) (P(VDF)) and amorphous poly(hexafluoropropylene) (P(HFP)) units. The mechanical strength of this copolymer primarily comes from the P(VDF) portion, while the P(HFP) portion contributes to the amorphous phase, which helps in trapping liquid electrolytes and facilitating the process of ionic conduction. This polymer matrix is well-suited as a host material for gel polymer electrolytes due to its ability to absorb liquid effectively while maintaining good mechanical stability. Additionally, P(VdF-HFP) has a high dielectric constant ($\varepsilon \approx 8.4$), making it suitable for solvating more salts, thereby enhancing ionic conduction in polymer electrolytes.

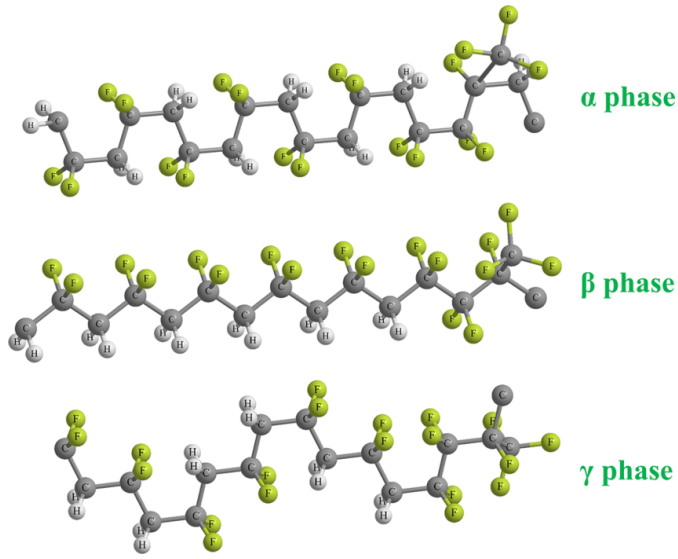


Fig 1.8 Three different phase structures of PVDF-HFP

The dissolution of salt within a polymer matrix involves the solvation of cations, anions, or both. For effective solvation in a polymer matrix, a salt should possess the following characteristics:

- Low lattice energy.
- Smaller cationic size and larger anionic size.
- Low charge density of the anion to minimize the formation of ion pairs.

Cation solvation occurs primarily due to electron pairs present on heteroatoms like ether (-O-), sulfide (-S-), phosphorous (-P-), amine (-N-), carbonyl (-C=O), and cyano (C=N) groups. Anion solvation typically involves hydrogen bonding or interactions with Lewis acids. In most polymer salt complexes, cations form complexes with the polymer backbone, while anions should have minimal interactions with both the polymer backbone and cations, allowing them to move freely within the polymer matrix.

The solubility of salts in polymer matrices is often analyzed in terms of Lewis acid-base interactions, following the hard/soft acid base (HSAB) principle proposed by Pearson and further elaborated by Bruce et al. According to this principle, the strongest interactions occur between hard acids (small cations with no valence electrons) and hard bases (non-polarizable ligands of high electronegativity), or between soft acids (large cations with easily polarizable or removable valence electrons) and soft bases (more polarizable

groups).

The most commonly studied cations in polymer-salt complexes follow a rough order from hard acids to soft acids: Mg^{2+}, Ca^{2+} > Li^{+}, Na^{+} > Ni^{2+}, Cu^{2+}, Zn^{2+} > Cd^{2+}, Ag^{+}, Hg^{2+}. The electron-donating hard Lewis bases in the polymer matrix have low polarizability and high electronegativity, forming strong complexes with hard Lewis acid-base small cations lacking valence electrons. Anions generally have weaker interactions with the Lewis base of the polymer matrix.

Salts with large monovalent anions, such as ClO^{4-}, BF^{4-}, CF_3SO3^{-}, (CF3SO2)2N-, PF6-, AsF6-, and SCN-, are well-suited for polymer matrices due to their low lattice energies and tendency to have slight ion pairing, especially those with large and flexible anions like those found in lithium super-acid salts, particularly the imide family salts. These larger anions can also have a plasticizing effect on the polymer.

Polymer Electrolytes with embedded Ionic Liquid:

Ionic liquids (ILs) have recently garnered significant interest among researchers as novel electrolyte materials or components due to their potential to enhance electrochemical performance. At room temperature, ILs are molten salts typically composed of bulky, asymmetric organic cations and inorganic anions. Unlike inorganic salts, which require solvation by a solvent to dissociate into ion pairs, ILs exist as completely dissociated ion pairs in the liquid state at room temperature. Incorporating ILs into polymer matrices is a promising technique to improve the physicochemical and electrochemical properties of polymer electrolytes. ILs possess several excellent properties that make them potential candidates for various electrochemical devices, including bioscience, biomechanics, and electrodeposition. Their physicochemical properties can be highly tuneable due to the wide variety of cation and anion combinations, making ILs often referred to as "designer solvents." However, most ILs suffer from drawbacks such as high viscosity, low ionic conductivity, and high cost, which can limit their practical application in electrochemical devices.Based on their composition, ILs can be classified into aprotic, protic, and zwitterionic types. Imidazolium-based ILs typically offer higher ionic conductivity, while pyrrolidinium-based ILs exhibit a wide electrochemical stability window (ESW). Cations such as imidazolium, pyrrolidinium, piperidinium, and quaternary ammonium have received significant attention for battery and supercapacitor applications. The electrochemical performance of

supercapacitors is also influenced by the viscosity and ion size of ILs.

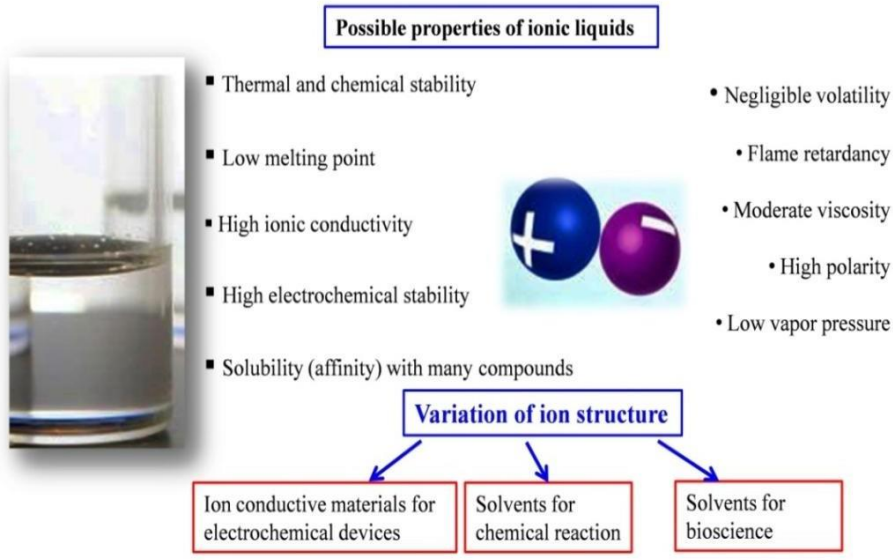


Fig 1.9 . Ionic Liquids and its significant Properties

In many cases, the solubility of lithium salts in ILs with the same anion is higher than in systems with different anions. Introducing ILs into polymer matrices decreases the glass transition temperature (Tg) and melting temperature (Tm) of the host polymer matrix. The

additional anions provided by ILs may act as coordinating bridges for lithium ions between polymer backbone chains and hinder the formation of crystalline polymer-salt phases. The presence of ILs in the polymer matrix serves as both plasticizers and additional sources of free ions for conduction. Moreover, the anions from ILs assist in partially or fully freeing lithium ions by interacting with the coordination between lithium ions and groups of the host polymer matrix, thereby increasing the number of charge carriers and improving charge transportation.

Gel Polymer Electrolytes

Gel polymer electrolytes (GPEs) represent a crucial category of ionic materials with significant practical applications. Typically, GPEs are formed by incorporating liquid electrolytes into a host polymer matrix, combining the ionic conductivity of liquids with the dimensional stability of solids. This offers advantages over both liquid and solid electrolytes,

addressing issues like low ionic conductivity in solid polymer electrolytes and evaporation and leakage problems in liquid electrolytes.

Essentially, GPEs comprise host polymer matrices, solvents (plasticizers), and salts. The host polymers should possess key properties such as polarity, low glass transition temperature, and high amorphousness. Salts should be soluble in chosen plasticizers, have large anion groups, and low dissociation energy. Meanwhile, solvents (plasticizers) should exhibit properties like high dielectric constant to enhance salt dissociation, low viscosity for high ionic mobility, high boiling point to prevent solvent evaporation, low freezing point to maintain conductivity at low temperatures, and presence of chemically active dipoles like the carbonyl group to induce high polarity.

In addition to these essential properties, plasticizers should also demonstrate thermal and electrochemical stability, good chemical compatibility with electrodes, and effective plasticizing effects. GPEs typically exhibit ionic conductivity greater than 10-3 S/cm, enabling fast charge transfer at electrode interfaces.

Various thermoplastic polymer matrices such as poly(methyl methacrylate) (PMMA), poly(acrylonitrile) (PAN), poly(vinylidene fluoride) (PVdF), and poly(vinylidene fluoride-co-hexafluoropropylene) (PVdF-HFP) are utilized as frameworks for GPEs. A range of salts including NH_4BF_4, NH_4PF_6, NH_4SCN, $LiPF_6$, $LiBF_4$, $LiCF_3SO_3$, $LiN(CF_3SO_2)_2$, and acids like

H_3PO_4 and HCF_3SO_3 are employed for ion conduction. Various solvents (plasticizers) such as EC, PC, DMC, and PEG are also used.

Plastic crystalline succinonitrile (SN) has recently emerged as a solid solvent or plasticizer in GPEs, enhancing ionic mobility due to its high dielectric constant and polar character. Additionally, ionic liquids have attracted attention for GPE preparation due to their unique properties. Copolymer P(VdF-HFP) and a variety of ionic liquids-based GPEs find application in rechargeable batteries, dye-sensitized solar cells, electric double-layer supercapacitors, thin-film transistors, among other electrochemical devices.

- **Electric Conductivity**

Polarization in Polymer Electrolyte

Electric polarization refers to the phenomenon where the positive and negative charges within atoms or molecules, or the orientation of existing dipoles, are displaced in response to an external electric field. This displacement results in a redistribution of charges within the material. There are four main types of electric polarization:

1. Electronic polarization: This occurs when the distribution of electron clouds around atoms or molecules is shifted from their equilibrium positions, creating an induced dipole moment. Electronic polarization is rapid and typically occurs in the visible or ultraviolet range of the electromagnetic spectrum.

2. Atomic or ionic polarization: Here, the applied electric field causes atoms or ions within a polyatomic molecule to shift relative to each other, generating an induced dipole moment. This type of polarization is associated with the ferroelectric effect and dipolar polarization, with a resonance frequency in the infrared range.

3. Orientational polarization: This occurs in dielectric materials with permanent dipole moments, where the electric field causes the reorientation of dipoles along its direction.

4. Space charge polarization: Mainly observed in amorphous or polycrystalline solids, space charge polarization arises from the separation of mobile charged particles under an applied

electric field. This separation creates positive and negative space charges within the material, affecting its dielectric constant. Two mechanisms, hopping polarization and interfacial polarization, contribute to space charge polarization.

In polymer electrolytes, contributions to polarization primarily come from orientational polarization, due to the flexible nature of polymer chains, and space charge polarization, resulting from the presence of charge carriers. Additionally, electrode polarization occurs due to the accumulation of charge carriers at the electrode-electrolyte interface, influencing the material's electric field and conductivity characteristics. These polarization processes exhibit time dependence and are influenced by factors such as temperature and the frequency of the applied electric field.

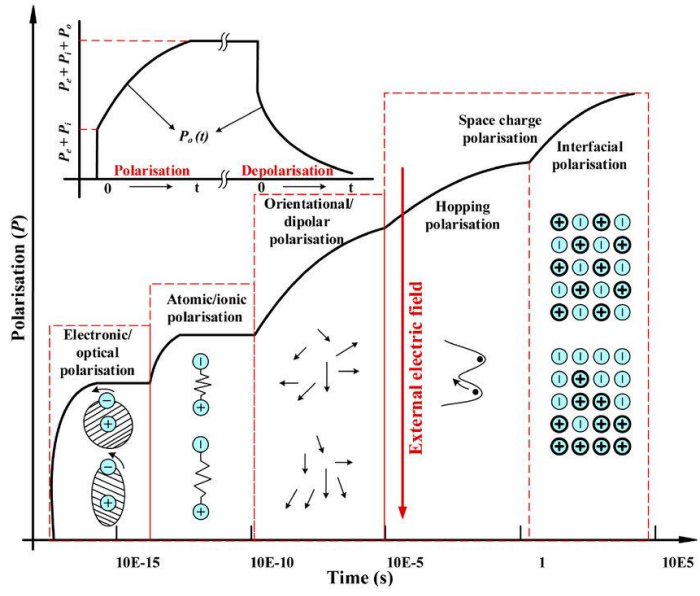


Fig 1.10. Basic Electric Polarization under unit step Electric Field

(a) Hopping polarization: This phenomenon occurs in dielectric materials when localized charges, such as charge carriers or vacancies (electrons and holes), are able to move or "hop" from one site to another nearby favourable site. As a result, hopping polarization emerges within the material.

(b) Interfacial polarization: Interfacial polarization arises from the accumulation of charge at the interface between two materials or regions within a material following the application of an electric field. This polarization occurs either in compound dielectrics or when two electrodes are connected to a dielectric material.

Complex Conductivity Spectra

To delve into the dynamics and relaxation of charge carriers in polymer electrolytes, researchers often turn to **dielectric relaxation spectroscopy** (**DRS**), employing an alternating current (ac) electric field. This technique offers valuable insights into molecular-level behaviors and relaxation mechanisms.

When subjecting a dielectric material to an ac electric field E, the resulting displacement current D is linked to the applied field by D = ε*E, where ε* represents the complex dielectric permittivity. This displacement current, being material-specific, may not always

align with the applied electric field E. The complex dielectric permittivity is expressed as:

$\varepsilon^*(\omega) = \varepsilon'(\omega) - i\varepsilon''(\omega)$

Here, $\varepsilon'(\omega)$ and $\varepsilon''(\omega)$ denote the real and imaginary parts of the complex dielectric permittivity, respectively. Moreover, the complex conductivity $\sigma^*(\omega)$ can be represented as:

$\sigma^*(\omega) = \sigma'(\omega) + i\sigma''(\omega)$

The frequency dependence of the real part of conductivity, σ', exhibits three distinct regions, each associated with different phenomena:

1. At low frequencies, σ' experiences a rapid decrease, primarily due to electrode polarization. This phenomenon arises from the motion of charge carriers but is considered non-equilibrium and extrinsic.

2. In the mid-frequency range, a frequency-independent conductivity (often denoted as σ_dc) is observed, indicating long-range ion diffusion through the polymer matrix via hopping between sites.

3. At high frequencies, σ' increases with frequency, with the dispersive region shifting towards higher frequencies as temperature increases. This shift signifies the onset of conductivity relaxation phenomena.

The imaginary part of conductivity, σ", follows a similar trend:

1. In the low-frequency region, σ" decreases as frequency decreases due to electrode polarization, reaching a maximum value at a certain frequency (ω ~ ω_max), indicating full development of electrode polarization.

2. In the mid-frequency region, σ" exhibits a minimum at a specific frequency (ω ~ ω_on), marking the onset of electrode polarization.

3. In the high-frequency region, σ" increases linearly with frequency. Both σ' and σ" increase with frequency in this region due to the primary contribution of dielectric relaxation of

dipoles in the host polymer matrix.

The linear frequency dependence of conductivity implies a regime where dielectric loss remains constant with frequency, known as the "Nearly Constant Loss" (NCL) regime. This regime is currently a topic of much debate and research interest in polymer electrolytes.

Charge Carrier Conduction Mechanism:

Investigating the mechanism of charge carrier conduction in polymer electrolytes offers valuable insights into their physicochemical properties, crucial from both fundamental and practical standpoints. In this section, we explore various analytical approaches to understand the microscopic dynamics of charge carriers.

Empirical Models:

Over the past decades, considerable research has focused on the electrical properties of disordered materials, with experimental findings analyzed to glean fundamental insights into material characteristics. This section elucidates several empirical models developed to dissect the electrical properties of ionic materials.

Jonscher Power Law:

The frequency dependence of the real part of complex conductivity, $\sigma'(\omega)$, in ionic conductors exhibits dispersive behaviour at high frequencies. The empirical Jonscher power law model provides a framework for analyzing the dynamics of charge carriers in polymer electrolytes. According to this model, conductivity $\sigma'(\omega)$ is expressed as:$\sigma'(\omega) = \sigma_{dc} + A\omega^n$

Here, σ_{dc} represents the dc or ionic conductivity, A is a weakly temperature-dependent constant, and n is a power law exponent typically ranging between 0 and 1. Generally, n values fall between 0.4 and 0.7 for ionic conductors. This frequency-dependent dispersive behavior is prominent in ionically conducting glassy materials, conducting polymers, and amorphous semiconductors, often referred to as "universal dielectric response" or "first universality."

Assuming the hopping frequency corresponds to the crossover frequency, Almond and West deduced a power law expression:

$$\sigma'(\omega) = \sigma_{dc}\,[(1 + \frac{\omega}{\omega_c})^n]$$

Here, ω_c denotes the crossover or hopping frequency, where $\sigma'(\omega_c) = 2\sigma_{dc}$. The exponent n, usually less than unity, is sometimes associated with the dimensionality of the conduction space.

Double Power Law

It is observed that at very low temperatures or high frequencies, experimental AC conductivity spectra across a broad range of temperatures and frequencies often deviate from fitting Almond-West power law relations. Consequently, an additional term is incorporated into the power law, leading to the double power law equation:

$$\sigma'(\omega) = \sigma_{dc}\,[(1 + \frac{\omega}{\omega_c})^n] + B\omega$$

Here, B represents a weakly temperature-dependent constant. This supplementary term, roughly proportional to frequency, introduces linear frequency dependence. This modified

power law equation effectively elucidates conductivity spectra across wider frequency and temperature ranges and introduces the concept of nearly constant loss (NCL).

Analyzing AC conductivity spectra using either the Almond-West power law or the double power law facilitates the determination of ionic conductivity and crossover frequency at specific temperatures. The temperature dependence of ionic conductivity σ_{dc} and crossover frequency ω_c can be elucidated using Arrhenius or Vogel-Tammann-Fulcher (VTF) relations.

Arrhenius and Vogel-Tammann-Fulcher (VTF) Relations:

While the Arrhenius relation traditionally describes the temperature dependence of dc/ionic conductivity in disordered solids, the experimental data for polymer electrolytes often deviates from this equation. Instead, the Vogel-Tammann-Fulcher (VTF) relation better fits the temperature-dependent dc conductivity data. This relation, originally developed to

describe the viscosity of supercooled liquids, is expressed as:

$$\sigma_{dc} = \sigma_0 \exp\left(\frac{-E_a}{k_B\, T - T_0}\right)$$

Here, T_0 represents the Vogel temperature or the equilibrium glass transition temperature. The VTF relation suggests that at $T=T_0$, excess configuration entropy becomes zero, indicating a halt in ion mobility. This empirical relation, along with the Stokes-Einstein relation for diffusivity of polymers and the Nernst-Einstein expression, provides a mathematical description of conductivity behaviour.

$$\eta_{dc} = \eta_0 \exp\left(\frac{-E_a}{k_B\, T - T_0}\right)$$

The difficulty in experimentally determining T_0 suggests it to be 50-100 K below the glass transition temperature T_g, which can be determined from differential scanning calorimetry (DSC) experiments. The VTF equation effectively describes the diffusion of uncharged molecules through disordered materials like polymer electrolytes, indicating its utility in understanding charge carrier dynamics and transport mechanisms.

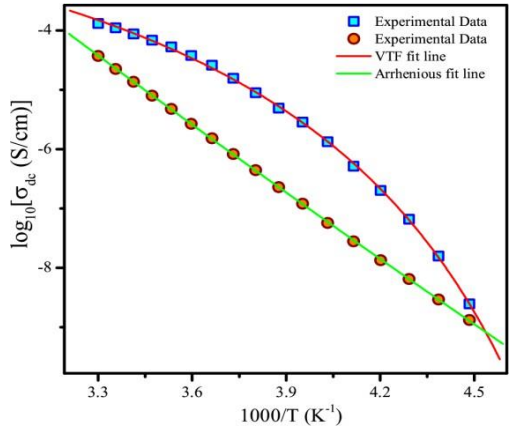


Fig.1.11 Temperature dependence of dc conductivity showing Arrhenius type behavior and VTF type behavior

Universality:

The ac conductivity spectra demonstrate two distinct phenomena known as universalities. The first, termed Universal Dielectric Response (UDR), typically manifests at high temperatures or in the low-frequency range of the conductivity spectra. Conversely, the

second, referred to as nearly constant loss (NCL), occurs at very high frequencies or in low-temperature conditions.

1st Universality: Universal Dielectric Response

Typically, the ac conductivity spectrum exhibits dispersion at high frequencies, presenting an opportunity to understand the interaction between ion conduction mechanisms and structural defects. This dispersive behavior can be mathematically described using the Jonscher power law, initially proposed by Jonscher to explain a broad range of disordered materials, termed the "Universal Dielectric Response" (UDR). In this context, the imaginary part of the complex dielectric permittivity ε" associated with UDR behavior is expressed as:

$$\boldsymbol{\varepsilon}^{"} = \left[\frac{\boldsymbol{\sigma'(\omega)-\sigma(0)}}{\boldsymbol{\varepsilon_0\omega}}\right] = \left(\frac{\boldsymbol{A}}{\boldsymbol{\varepsilon_0}}\right)\boldsymbol{\omega}^{-(1-n)}$$

Here, ε_o represents the dielectric permittivity in vacuum, and σ' denotes the ac conductivity as a function of angular frequency. Both A and σ(0) are thermally activated parameters. Moreover, the real part of the complex dielectric permittivity ε" can be derived from the Kramers-Kronig (K-K) relation.

$$\boldsymbol{\varepsilon'} = \boldsymbol{\varepsilon_\propto} + \frac{\boldsymbol{A}}{\boldsymbol{\varepsilon_0}}\boldsymbol{\tan}\left(\frac{\boldsymbol{n\pi}}{\boldsymbol{2}}\right)\boldsymbol{\omega}^{-(1-n)}$$

2nd Universality: Nearly Constant Loss (NCL):

The ac conductivity σ'(ω) exhibits nearly linear variation with frequency and shows minimal dependence on temperature, particularly at low temperatures or high frequencies. This behavior is expressed as:

$$\boldsymbol{\sigma_{NCL}(\omega) = A\varepsilon_0\omega}$$

Here, A is a constant with weak temperature dependence, and ε_0 represents the dielectric permittivity in vacuum. This relationship signifies a secondary regime of ac conductivity termed the nearly constant loss (NCL) regime. In this regime, the dielectric loss, $\varepsilon"(\omega) = \sigma'_{NCL}(\omega)/\omega\varepsilon_0 \approx A$, remains nearly frequency-independent. The NCL phenomenon is

observed predominantly in glassy and disordered ionic conductors. However, its precise origin remains subject to debate.

Different viewpoints suggest various origins for the NCL response:

1. Some propose that NCL arises from collective movements of atom groups in asymmetric double well potential configurations.

2. Others suggest that it may stem from the vibrational motion of ions within slowly decaying anharmonic cages in ionic conductors.

3. Another viewpoint suggests that NCL behavior results from the hopping movements of mobile charge carriers between neighboring sites.

While the NCL phenomenon is observed in various disordered ion conducting glasses and ceramics, its occurrence in ion conducting polymer electrolytes lacks a universally accepted explanation. Moreover, the frequency and temperature range of the NCL response are influenced by factors such as ion concentration and polymer chain flexibility.

Bibliography:

[1] R. P. Feynman, A lecture in engineering science, In California Institute of Technology,Feb. edn.

[2] P. Motiarty, Rep. Prog. Phys. 64 (2001) 297.

[3] Kuo-Feng Lin, Hsin-Ming Cheng, Hsu-Cheng Hsu, Li-Jiaun Lin, Wen-Feng Hsieh,

[4] Chemical Physics Letters 409 (2005) 208–211

[5] O. Vigil, F. Cruz, A. Morales-Acevedob, G. Contreras-Puente, Materials Chemistry and Physics 68 (2001) 249–252

[6] C. Fasciani, S. Panero, J. Hassoun and B. Scrosati, *Journal of Power Sources* (2015), p. 180.

[7] D. M. a. H. S. K. Bruce Bagley The Impact of Emerging Economies on Global Energy and the Environment, Lexington Books, Lanham (2015).

[8] M. Que, Y. Tong, G. Wei, K. Yuan, J. Wei, Y. Jiang, H. Zhu and Y. Chen, *J. Mater. Chem. A* **4** (2016), p. 14132.

[9] F. Béguin, V. Presser, A. Balducci and E. Frackowiak, *Adv. Mater.* **26** (2014),p. 2219.

[10] V. L. Martins, A. J. R. Rennie, R. M. Torresi and P. J. Hall, *Phys. Chem. Chem. Phys.* **19** (2017), p. 16867.

[11] M. Winter and R. J. Brodd, *Chem. Rev.* **104** (2004), p. 4245.

[12] S. Holmberg, A. Perebikovsky, L. Kulinsky and M. Madou, *Micromachines* **5** (2014), p. 171.

[13] D. P. Dubal, O. Ayyad, V. Ruiz and P. Gomez-Romero, *Chemical Society Reviews* **44** (2015), p. 1777.

[14] J. Nunes-Pereira, C. M. Costa and S. Lanceros-Méndez, *Journal of Power Sources* **281** (2015), p. 378.

[15] B. Scrosati, Modern Batteries (Second Edition), Butterworth-Heinemann, Oxford (1997).

[16] G.-L. Xu, Q. Wang, J.-C. Fang, Y.-F. Xu, J.-T. Li, L. Huang and S.-G. Sun, *J. Mater. Chem. A* **2** (2014), p. 19941.

[17] K. Shehzad, Y. Xu, C. Gao and X. Duan, *Chemical Society Reviews* **45** (2016), p. 5541.

Chapter 2:

Literature Review

Review of Past Work:

After World War II, the industrialized world witnessed unprecedented economic growth, fuelled in part by advancements in the chemical sciences, particularly in polymer materials. These materials ranged from classic synthetic polymers like polyolefins and polyacrylics to innovative inorganic polymers such as polysiloxanes and polyphosphazenes. Additionally, modern synthetic resins like epoxy, polyurethane, and polyester played significant roles.

During this period, physicochemical and theoretical tools emerged to study polymer properties, leading to a better understanding of their structural, mechanical, and transport characteristics. Observations such as lamellar crystallinity, morphologies like spherulites and fibres, and the entropic nature of rubber elasticity were elucidated, notably by Flory's work on random-coil configurations.

In **1998**, Wright categorized the history of polymer electrolytes into periods, starting with the post-World War II "classic period" and transitioning into a "period of change" in the early 1970s, marked by events like the 1973 oil crisis. This crisis prompted a re-evaluation of energy infrastructure and production methods, driving the need for innovative solutions, including polymer electrolytes, for energy storage and conversion.

By the mid-1970s, there was scepticism about significant new discoveries in polymer synthesis for consumer applications, leading research focus to shift towards fields like composite materials and high-performance fibres such as Kevlar. Additionally, advancements in solid-state physics and chemistry were sought to understand electroactive and optically active polymers, necessitating multidisciplinary efforts spanning organic chemistry, physical chemistry, and device engineering.

The polymer electrolytes are first studied by **P. V. Wright** [1] in **1973** and coworkers and M. B. Amrand and co-workers established their wide potential to be used as separator/electrolyte materials for energy storage/conversion devices in 1978. Therefore, these polymer electrolytes have a wide history of more than four decades now. Over the long time, these materials have evolved and specific researches are carried out to overcome their several limitations. The main reason for extensive research on these types of materials is conductivity behaviour of these materials which is ionic in nature. A comprehensive discussion will be portrayed in the following sections on different classes of polymer electrolytes and numerous techniques are adopted to improve their physicochemical properties for practical applications in energy

storage/conversion devices.

The synthesis and exploration of poly-ethers have been extensively documented for their remarkable coordinating capabilities, as seen in studies detailing molecular complexes between polyethylene oxide (PEO) and substances like mercury chloride. In 1973, Fenton, Parker, and Wright observed the semicrystalline structure of complexes between PEO and alkali salts, which laid the groundwork for subsequent investigations into their electrical properties and ion conductivity.

Armand's proposal in 1970s to use these systems as solid polymer electrolytes for lithium batteries sparked widespread research interest. Throughout the 1980s, as microelectronics and portable devices gained prominence, there was a growing demand for lightweight, high-performing, and affordable secondary batteries, driving significant advancements in polymer electrolytes. Strategies were devised to suppress crystallinity in these materials, which was found to impede ionic conductivity.

The **1990s** saw the proliferation of lithium-ion batteries and the mass production of portable electronics, further propelling research into polymer electrolytes. Novel electrolyte systems such as "salt-rich" or Angell's "polymer-in-salt" electrolytes emerged, alongside gel electrolytes incorporating solvent molecules. Solvent-free polymer electrolytes remained crucial for both research and practical applications, with a focus on single-ion conduction systems and low-dimensional structures to enhance ion mobility.

In the new millennium, hybrid inorganic-organic polymer electrolytes have emerged as promising candidates for high-performance lithium secondary batteries due to their mechanical, thermal, chemical, and electrochemical stability, along with high room temperature conductivity. Research efforts have delved into understanding the role of host polymer crystallinity on ion-conducting mechanisms, leading to the development of diverse materials including those incorporating inorganic species or ionic liquids.

The expanding array of innovative materials reflects the growing demand for energy conversion and storage devices such as secondary batteries, fuel cells, supercapacitors, sensors, dye-sensitized solar cells, actuators, and microelectronic devices. Polymer electrolytes stand as essential components driving advancements in this field, poised to play a pivotal role in future

scientific and technological landscapes.

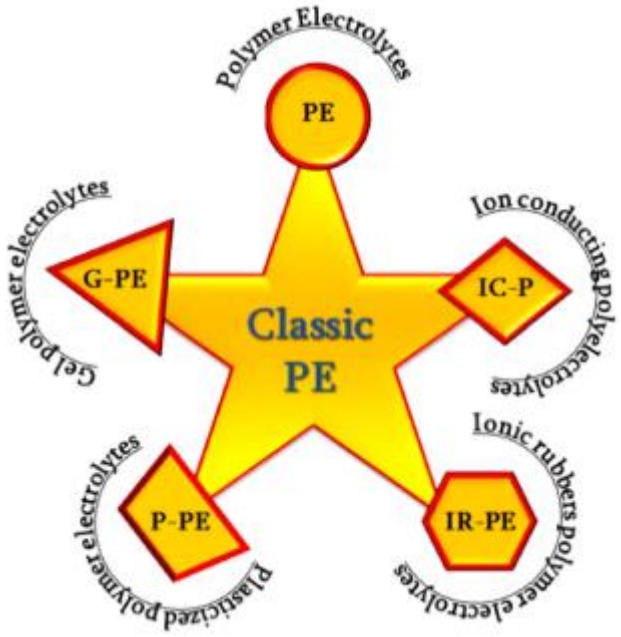


Fig. 2.1 Classification of Polymer Electrolytes [18]

In **2000** B.W. Ricketts *et al.* [19] discussed the self-discharge characteristics of carbon-based supercapacitors utilizing organic electrolytes. He examined the diffusion of ions from areas of heightened ionic concentration generated during the capacitor's charging phase. He also studied the phenomenon of charge leakage across the double-layer at the interfaces between the electrolyte and carbon components within the capacitor. The study outlines the influence of temperature and initial voltage levels across the capacitor on the self-discharge rate.

In **2007** J.D. Kim *et al.* [20] investigated, a molecular hybrid conductor electrolyte was synthesized by combining PWA with ([BMIM][TFSI]) ionic liquid. The [BMIM][TFSI] ionic liquid exhibited an affinity for the strongly acidic PWA, facilitating interaction between the two components. These hybrids displayed a hydrophilic nature, incorporating water molecules within their structure. Even at elevated temperatures up to 80 °C, the water molecules remained within the hybrids, contributing to enhanced conductivity under an anhydrous N2 atmosphere. Specifically, the conductivity of the PWA-[BMIM][TFSI] hybrid increased from 10−4 S/cm to 0.04 S/cm at 60 °C under anhydrous conditions. Notably, the conductivity of the hybrids at each temperature surpassed that of pure PWA and [BMIM][TFSI] under similar anhydrous conditions, likely attributed to the presence of protonic carriers within the hybrids.

In **2011** H. Yu et al. [21] reported that a quasi-solid-state supercapacitor was constructed using alkaline polyvinyl alcohol and potassium iodide (PVA–KOH–KI) as the gel electrolyte, paired

with activated carbon electrodes. The electrochemical properties of this supercapacitor were assessed using cyclic voltammetry, galvanostatic charge–discharge, and electrochemical impedance spectroscopy techniques. Incorporating KI into the electrolyte was found to enhance its ionic conductivity while improving the pseudo-capacitance of the electrodes.

The specific capacitance of the supercapacitor was measured at 236.90 F g−1, representing a notable 74.28% increase compared to the PVA–KOH system under the same current density conditions. Furthermore, the energy density and power density of the supercapacitor were determined to be 7.80 Wh kg−1 and 15.34 kW kg−1, respectively. Importantly, the supercapacitor exhibited excellent cycle-life stability, indicating its potential for long-term and reliable energy storage applications.

In **2014** J.P. Tafur *et al.*, [22]developed Gel Polymer Electrolytes (GPEs) by incorporating three different ionic liquids (ILs) - 1-ethylpyridinium bis(trifluoromethylsulfonyl)imide (EPy TFSI), 1-ethyl-3-methylimidazolium bis(trifluoromethylsulfonyl)imide (EMIM TFSI), and trihexyltetradecylphosphonium bis(trifluoromethylsulfonyl)imide ($P_{6,6,6,14}$ TFSI) - with the same anion, TFSI−, into the host polymer poly(vinylidene fluoride-co-hexafluoropropylene) (PVdF-HFP). These additions, with or without $ZnTf_2$ salt, resulted in GPEs. Compared to pristine PVdF-HFP films, the incorporation of IL or IL+$ZnTf_2$ salt led to the formation of more amorphous and ionic membranes. The characteristics such as ionic conductivity values, impedance spectra, dielectric measurements, voltammograms, and potential stability were found to be dependent on the type of IL cation used in the GPE. Additionally, the presence of $ZnTf_2$ salt within the film enhanced the ionic conductivity across all GPEs, likely due to the presence of free triflate anions. The involvement of Zn^{2+} cations in the conduction process was confirmed through cyclic voltammetry and EDX measurements.Among the six GPEs investigated, the PVdF-HFP+EMIM TFSI+ZnTf2 membrane demonstrated the most promising outcomes: it exhibited a maximum value of ionic conductivity (1.73×10−1 S m−1), low activation energy value, and displayed highly reversible and high current density voltametric behaviour.

In **2018**, P. Pal *et al.* [23]studied the physicochemical properties of gel polymer electrolytes based on poly(vinylidene fluoride-hexafluoropropylene) embedded with different ionic liquids, namely 1-butyl-2,3-dimethylimidazolium tetrafluoroborate, 1-butyl-3-methylimidazolium tetrafluoroborate, and 1-ethyl-3-methylimidazolium tetrafluoroborate, aiming to utilize them in electrochemical devices such as electrochemical capacitors. It was found that the size and viscosity of cations, as well as the dielectric constant of the ionic liquids, influence the physicochemical properties and electrochemical stability of the gels, and subsequently affect the

electrochemical performance of the electrochemical capacitors fabricated with these gel electrolytes. Through cyclic voltammetry, galvanostatic charge-discharge, and electrochemical impedance spectroscopy, the electrochemical performance of the capacitors was evaluated. It was found that the gel electrolyte embedded with 1-ethyl-3-methylimidazolium tetrafluoroborate ionic liquid, characterized by the smallest cation size and highest ionic conductivity, demonstrates promising physicochemical properties. Moreover, it performs well as an electrolyte/separator in devices, exhibiting favourable specific capacitance, energy density, and cycle life compared to others.Specifically, the electrochemical capacitor assembled with 1-ethyl-3-methylimidazolium tetrafluoroborate doped gel electrolytes showcases a specific capacitance of 113.6 F g−1, equivalent series resistance of 20 Ω-cm2, energy density of 17.48 Wh kg−1, response time of 5.46 s, and pulse power of 7.19 kW kg−1 at a current of 1.0 mA cm−2, highlighting its favorable performance characteristics.

In **2022**, SA Hashmi *et al*. [24] reported that a novel non-aqueous, redox-active GPE composed of an ionic liquid, 1-ethyl-3-methylimidazolium bis(trifluoromethylsulfonyl)imide, augmented with KI additive, immobilizes within a poly(vinylidene fluoride-co-hexafluoropropylene) matrix. The optimized GPE composition exhibits flexibility, outstanding mechanical and thermal stabilities, high ionic conductivity (3.9 × 10−3 S cm-1 at room temperature), and broad electrochemical stability (∼5.05 V versus Ag). Utilizing this redox-active GPE, a carbon supercapacitor is fabricated with symmetrical electrodes composed of porous activated carbon derived from waste biomass pollen cones. The inclusion of KI in the GPE induces rapid redox activity at the AC-electrode/GPE interfaces, thereby significantly enhancing capacitance (from ∼115 to ∼250 F g−1) and energy (from ∼31 to ∼65 Wh kg−1) at a maximum power of 34–36 kW kg−1. Moreover, the supercapacitor featuring the redox-active GPE demonstrates satisfactory self-discharge behaviour and cycling performance, exhibiting only ∼11% initial fading.

In **2023** Subir Kumar Patla *et al*. [25] synthesized using poly(vinylidene fluoride-co-hexafluoropropylene) as the host polymer, adiponitrile as a plasticizer, and 1-ethyl-3-methylimidazolium bis(trifluoromethylsulfonyl)imide as the ionic liquid (IL). Additionally, diphenylamine (DPA) and copper iodide (CuI) were employed as dual redox additives. Microstructural analysis revealed that the inclusion of plasticizers, ILs, and redox additives promoted the amorphous character of the host polymer matrix. The thermal stability of the

GPEs was demonstrated up to approximately 200 °C. The electrical conductivity at room temperature and the electrochemical potential window of the dual redox additive-based GPE containing IL, DPA, and CuI were measured at 3.3 × 10–3 S cm^{-1} and 6.4 V, respectively. Supercapacitors (SCs) were assembled using the dual redox additive-based GPEs and activated carbon (AC) electrodes, and their electrochemical performance was assessed through cyclic voltammetry, galvanostatic charge–discharge, and electrochemical impedance spectroscopy. Results indicated that the incorporation of dual redox additives significantly increased the specific capacitance from 108.3 to 243.4 F g^{-1} and the specific energy from 5.1 to 11.5 W h kg^{-1}. Furthermore, the dual redox additive-based GPEs exhibited robust cyclic performance, with an initial 34% capacitance fading and sustained Coulombic efficiency of approximately 100% over 5000 cycles.

Bibliography:

[1] P.V. Wright, Electrochim. Acta 43 (1998) 1137.

[2] D.E. Fenton, J.M. Parker, P.V. Wright, Polymer 14 (1973) 589.

[3] P.V. Wright, Brit. Polym. J. 7 (1975) 319.

[4] P.G. Bruce, C.A. Vincent, New Polym. Mater. 2 (1990) 19.

[5] P.V. Wright, J. Polym. Sci., Polym. Phys. Ed. 14 (1976) 955.

[6] M.B. Armand, J.M. Chabagno, M. Duclot, in: P. Vashisha, J.N. Mundy, G.K. Shenoy (Eds.), Fast Ion Transport in Solids, 1979, p. 131, North Holland, New York.

[7] A. Killis, J.F. LeNest, H. Cheradame, Makromol. Chem. Rapid 1 (1980) 595.

[8] C.C. Lee, P.V. Wright, Polymer 23 (1982) 681.

[9] D.R. Payne, P.V. Wright, Polymer 23 (1982) 690.

[10] D.J. Bannister, G.R. Davies, I.M. Ward, J.E. McIntyre, Polymer 25 (1984) 1600.

[11] P.M. Blonsky, D.F. Shriver, P. Austin, H.R. Allcock, J. Am. Chem. Soc. 106 (1984) 6854.

[12] C.V. Nicholas, D.J. Wilson, C. Booth, J.R.M. Giles, Brit. Polym. J. 20 (1988) 289.

[13] M.A. Ratner, in: J.R. MacCallum, C.A. Vincent (Eds.), Polymer Electrolyte Reviews Ch. 7, vol. 1, Elsevier, London, 1987.

[14] M.A. Ratner, A. Nitzan, Faraday Discuss. Chem. Soc. 88 (1989) 19. [15] C.A. Angell, Solid State Ionics 9–10 (1983) 3.

[16] L.M. Torell, C.A. Angell, Brit. Polym. J. 20 (1988) 173.

[17] H. Cheredame, in: H. Benoit, P. Rempp (Eds.), IUPAC Macromolecules, Pergamon, New York, 1982, p. 251. [18] M. Watanabe, N. Ogata, in: J.R. MacCallum, C.A. Vince

[18] Polymer electrolytes: Present, past and future, Electrochimica. Acta 57 (2011) 4-13

[19] B.W. Ricketts, C. Ton-That, Journal of Power Sources Volume 89, Issue 1, July 2000, Pages 64-69

[20] Je-Deok Kim , Shigenobu Hayashi , Toshiyuki Mori , Itaru Honma, Electrochimica. Acta Volume 53, Issue 2, 1 December 2007, Pages 963-967

[21] Haijun Yu, Jihuai Wu, Leqing Fan, Kaiqing Xu, Xin Zhong, Youzhen Lin, Jianming Lin Electrochimica Acta,Volume 56, Issue 20, 1 August 2011, Pages 6881-6886

[22] Juan P. Tafur, Antonio J. Fernández Romero, Journal of Membrane Science Volume 469, 1 November 2014, Pages 499-506

[23] P. Pal, A. Ghosh Journal of Power Sources, Volume 406, 1 December 2018, Pages 128-140

[24] Abbas Ali Hor, Neetu Yadav, S.A. Hashmi Journal of Energy Storage Volume 47, March

2022, 103608

[25]SubirKumarPatla,PulakPal,andAswiniGhosh,ACSAppl.EnergyMater.2023,6,8989−9000

Chapter 3:

Sample Preparation Technique

Synthesis of Ionic Liquid based Gel Polymer Electrolytes with Redox Additives

- ## Brief History of Polymer Electrolytes

The polymer electrolytes are first studied by P. V. Wright in 1973 and coworkers and M. B. Amrand and co-workers established their wide potential to be used as separator/electrolyte materials for energy storage/conversion devices in 1978. Therefore, these polymer electrolytes have a wide history of more than four decades now. Over the long time, these materials have evolved and specific researches are carried out to overcome their several limitations. The main reason for extensive research on these types of materials is conductivity behaviour of these materials which is ionic in nature. A comprehensive discussion will be portrayed in the following sections on different classes of polymer electrolytes and numerous techniques are adopted to improve their physicochemical properties for practical applications in energy storage/conversion devices.

- ## Introduction

Gel Polymer Electrolytes are one of the most important classes of ionic materials used for a various purpose such as in supercapacitor coin cell battery de-synthesized solar cell thin film transitions etc. In general GPEs are obtained by trapping the liquid electrolytes in host polymer matrix which provides a solid like stability and liquid like high ionic conductivity. The disadvantages of liquid electrolyte such as evaporation and leakage problem are overcome by quasi-solid or gel like polymer electrolytes. Likewise, the low ionic conductivity in solid electrolyte can also be enhanced using gel polymer electrolytes. They are made up of solvent host polymer matrix and salts. The essential properties of host polymer matrix are polar in nature, low glass transition and highly amorphous etc. The essential characteristic of the salt are they should be soluble in the chosen plasticizer presence of large anions low dissociation energy etc. The solvents or plasticizers should have the following properties:

1) High dielectric constant which enhances the level of salt dissociation,
2) Low viscosity which leads to high ionic mobility
3) High boiling point essential to avoid evaporation within the set temperature range
4) Low freezing point
5) Presence of chemically active dipoles

The other essential properties of plasticizers are thermal and electrochemical stability good

chemical compatibility and good plasticizing effect of the plasticizers. A number of thermoplastic polymer matrices such as poly (methyl methacrylate) PMMA, Poly(acrylonitrile) PAN, Poly(vinylidene fluoride) PVdF and Poly(vinylidene fluoride co-hexafluoropropylene) (PVdF-HFP) etc. are projected as frameworks for GPEs. In this work we have used ionic-liquid based Gel polymer electrolytes with its application in electric double layer supercapacitor.

- **Polymer Electrolyte embedded with Ionic Liquids:**

  Ionic Liquids have received an exponential interest from most of the researchers as novel electrolyte component for better electrochemical performance At room temperature ionic liquids are at molten state and consist of bulk, asymmetric cation group and inorganic anion group. But there is some difference between ionic liquid and inorganic salt. The inorganic salts require solvation by a solvent to dissociate into an ion pair. But in Ionic Liquids we do not require solvation as they exist as ion pairs in liquid state at room temperature. Introduction of ionic liquid in the polymer matrix is the most promising technique to enhance the physiochemical and electrochemical properties of the polymer electrolytes. Ionic liquids have excellent properties which make them a good candidate for good electrochemical performance in devices

- **Plasticized Polymer Electrolytes:**

  Plasticization is one of the most important technique to increase the flexibility of the polymer backbone chains and the ionic conductivity of the polymer electrolyte by using various type of plasticizers having low molecular weight and non-volatile monomeric organic liquid. A wide variety of plasticizers are is used for plasticization process such as polyethylene glycol (PEG), adiponitrile (ADN), ethylene carbonate propylene carbonate etc. Plasticizers can easily create strong polar attractive forces with polymer backbone chains of polymer matrix due to very small size. The local chain flexibility increases due to addition of plasticizer.

- **Materials Used:**

  All chemicals such as polymer matrix, ionic liquids, solvents, carbon materials were used as received. The used chemicals are poly(vinyli-dene fluoride-hexafluoropropylene) P(VdF-HFP), (Mw ~ 455,000 g/ mol, Aldrich), polyvinylidenefluoride as a binder (PVdF, powder, MTI Crop.), (Mw~534,000 g/mol, Aldrich, (1-Butyl-3-methylimidazolium bis(trifluromethylsulfonyl) imide ionic liquid (BMIMTFSI, ≥98.0%, Aldrich), acetone (Merck purity ≥ 99.5%), N-methyl-2 pylorridone (NMP, analytical grade, Aldrich), acetylene carbon black (MTI Crop.), activated carbon (AC, TCI Chemicals, Japan), flexible graphite sheets with

0.5 mm thickness (NICKUNJ Eximp Entp P LTD), aluminum (Al) and copper (Cu) foil (MTI Crop.). The value of density of ionic liquid used i.e. BMIMTFSI obtained from Sigma Aldrich database is 1.2929 g cm^{-3} respectively. These chemicals were used without further purification. All ionic liquids were stored inside the argon gas filled glove box (mBRAUN LAB star ECO) with < 0.5 ppm H_2O and < 0.5 ppm O_2.

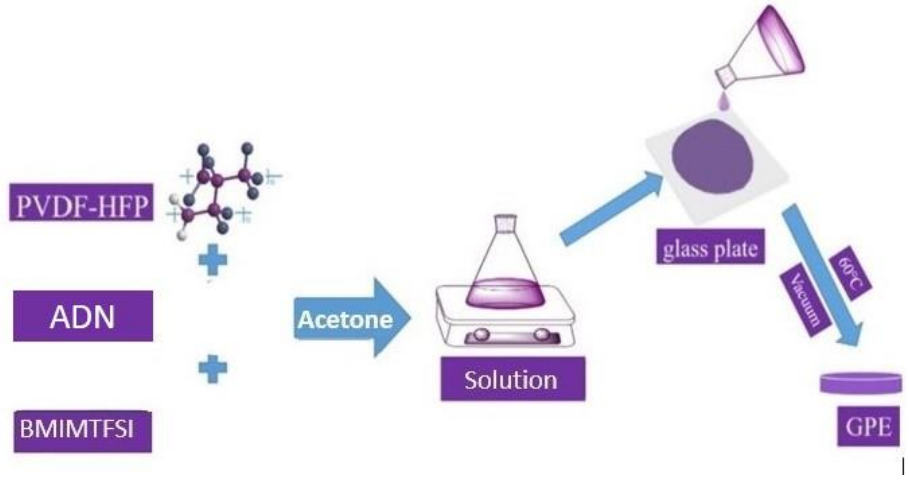


Fig 3.1 Schematic Diagram of the Experimental Process for the preparation of GPE

- ## Experimental Details:

Synthesis of Gel Polymer Electrolytes are done by cast solution technique. In our synthesis process we have taken a co-polymer Poly(vinylidene fluoride-*co*-hexafluoropropylene) i.e. (PVDF-HFP) (M.Wt. 455,000 g/mol) in a beaker of typical stochiometric weight. Now we add 10 ml of Acetone in the beaker and we place it on a heat-top magnetic stirrer at a temperature of 70° C and at a speed of 320 rpm. The granular PVDF-HFP starts to dissociate in the acetone to form a homogeneous mixture. Now we add ADN (Adiponitrile) plasticizers and Ionic Liquid i.e. BMIMTFSI (1-Butyl-3-methylimidazolium bis(trifluromethylsulfonyl) imide in typical stochiometric ratios with respect to the host co-polymer matrix. The weight ratio of PVDF-HFP ionic liquid and ADN is taken as 2:3:5. The ionic liquid and plasticizers were added using micro-pipped. Now the solution formed was allowed to stir for 2-3 hrs and cast into a clean petri-dish to get a free-standing film of thickness 0.25-0.35 mm by keeping it in a dry place in ambient condition for 24 hrs. We denote this as GPE 0. Now we prepare Gel Polymer Electrolytes based on redox additive.

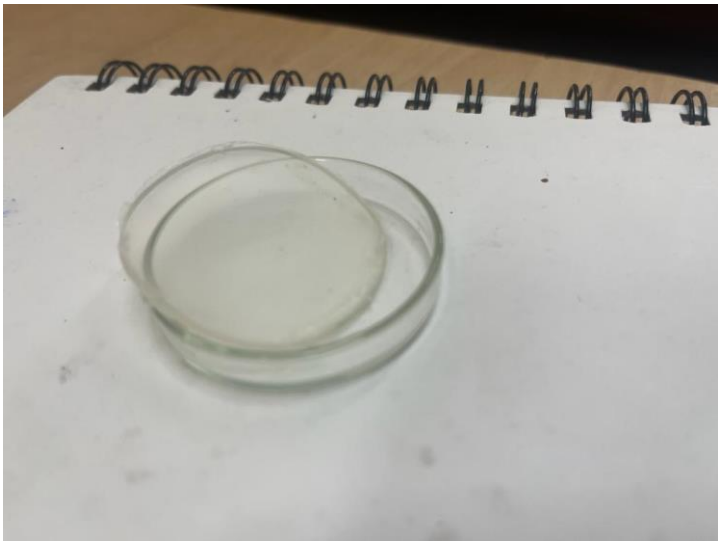


Fig 3.2. Synthesized Gel Polmer Electrolyte

Redox active Gel Polymer Electrolyte (GPE):

In the synthesis of gel polymer electrolyte, we follow the previous steps till the addition of ADN and Ionic Liquid. After the addition of ADN and Ionic liquid we allow the homogenous solution to be stirred for 1 or 2 more hours and after that we reduce the temperature to 60°Cand we add 40 mg of CsI (Cesium Iodide) which is almost 15 wt% of the host polymer matrix. Now we allow the homogeneous solution to be stirred for an hour after which we reduce the temperature to reduce the heat and after the beaker has achieved room temperature, we cast the solution into a petri-dish and allow it to dry overnight. We get a free-standing film of Gel Polymer electrolyte and name it as GPE-CsI. Now we repeat the same process for other redox additive such as RbI (Rubidium Iodide) and KI (Potassium Iodide) and name them as GPE-RbI and GPE-KI respectively.

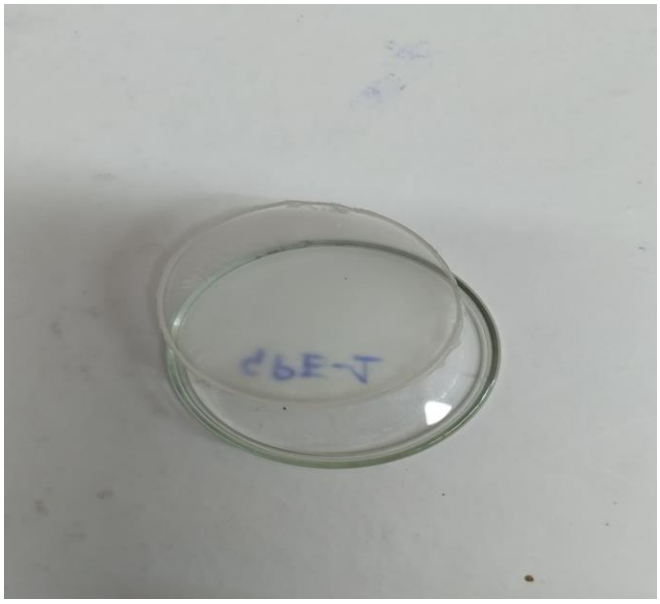


Fig 3.3. Synthesized Gel Polymer Electrolyte with redox-additive

- **Synthesis of Electrodes:**

The activated carbon (AC) and acetylene carbon black (CB) powders were kept in vacuum oven overnight at ~ 100 °C before use. Volumetric N_2 adsorption/desorption isotherm of the activated carbon (AC) was carried out by using Autosorb iQ station1 (quantachrome, USA) at 77 K to estimate the Brunauer-Emmett-Teller (BET) specific surface area and porosity at the relative pressure range of 0.022–1.0. The AC is degassed at 120 °C for 1 h in N_2 atmosphere. This isotherm shows almost type-1 isotherm signifying a large surface area from micro-pores. The BET specific surface area and porosity parameters of the AC are summarized in supplementary information. The specific surface area of the AC is ~633.53 m2 g−1, total pore volume is ~0.921 cm3 g−1 and average pore size is 1.83 nm. A brief sketch of electrode preparation was given as follows. A homogeneous slurry of activated carbon powder (AC), CB powder, P (VdF) as a binder in the ratio of 75:10:15 (wt/wt) was prepared by adding 400µl of DMF in the centrifuge tube where all the chemicals are taken. Now we have to stir the prepared solution for 1-2 hrs so that we get the homogeneous solution of the slurry before we undertake the coating process of the graphite sheet. The average cross-sectional area of the tip of the graphite sheet which is to be coated is almost equal to 1 cm^2. The tip of the graphite sheet of the specified area was coated with the slurry by drop-cast technique so that there is a uniform mass loading of 2 mg cm^{-3}. The electrodes prepared were dried overnight.

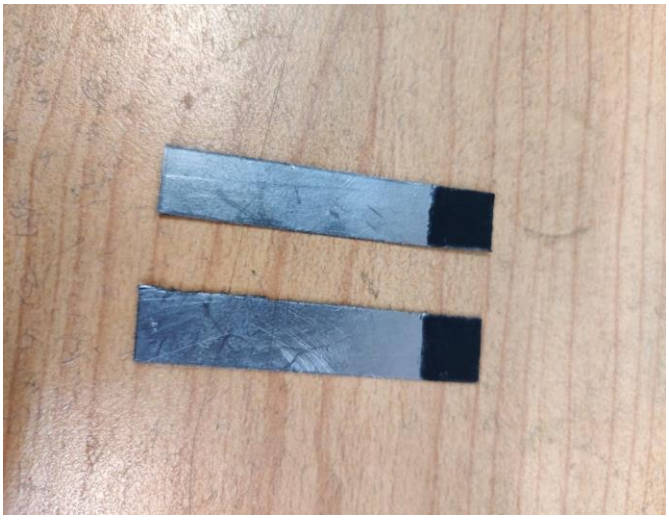


Fig 3.4. Synthesized graphite sheet electrodes

- ## Fabrication of Electric Double Layer Capacitance (EDLC):

An Electrochemical double layer capacitor was fabricated using the prepared gel polymer electrolytes sandwiched between the two graphite sheet electrodes coated with the prepared slurry. The gel polymer electrolyte acts as a self-separator. Now the prepared device was clipped together using glass slides and the device is now ready for conduction of electrochemical measurements such as Cyclic Voltammetry Galvanostatic Charge Discharge and Electrochemical Impedance Spectroscopy (EIS). We will study the aforesaid measurement techniques in forthcoming chapters. The prepared devices are:

Cell 1: AC||GPE-IL||AC

Cell 2: AC||GPE-CsI-40||AC

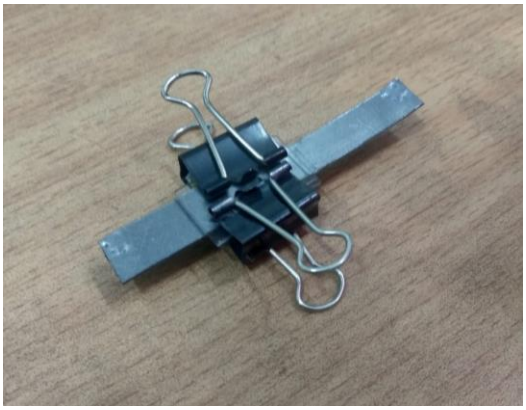


Fig3.5. Electrochemical Double Layer Capacitance (EDLC) fabricated using GPE and graphite electrodes

Bibliography:

[1] G.P. Pandey, S.A. Hashmi, Ionic liquid 1-ethyl-3-methylimidazolium tetracyanoborate-based gel polymer electrolyte for electrochemical capacitors, J. Mater. Chem. A 1 (2013) 3372–3378.

[2] J. Tian, C. Cui, Q. Xie, W. Qian, C. Xue, Y. Miao, Y. Jin, G. Zhang, B. Guo, EMIMBF4- GBL binary electrolyte working at -70 [degree]C and 3.7 V for a high performance graphene-based capacitor, J. Mater. Chem. A 6 (2018) 3593–3601.

[3] E. Frackowiak, F. Béguin, Carbon materials for the electrochemical storage of energy in capacitors, Carbon 39 (2001) 937–950.

[4] W. Deng, T. Kang, H. Liu, J. Zhang, N. Wang, N. Lu, Y. Ma, A. Umar, Z. Guo, Potassium hydroxide activated and nitrogen doped graphene with enhanced supercapacitive behavior, Sci. Adv. Mater. 10 (2018) 937–949.

[5] M. Brachet, T. Brousse, J. Le Bideau, All solid-state symmetrical activated carbon electrochemical double layer capacitors designed with ionogel electrolyte, ECS Electrochem. Lett. 3 (2014) A112–A115.

[6] C. Lin, L. Hu, C. Cheng, K. Sun, X. Guo, Q. Shao, J. Li, N. Wang, Z. Guo, NanoTiNb2O7/carbon nanotubes composite anode for enhanced lithium-ion storage, Electrochim. Acta 260 (2018) 65–72.

[7] Y. Guo, Y. Li, X. Lou, J. Guan, Y. Li, X. Mai, H. Liu, C.X. Zhao, N. Wang, C. Yan, G. Gao, H. Yuan, J. Dai, R. Su, Z. Guo, Improved extraction of cobalt and lithium by reductive acid from spent lithium-ion batteries via mechanical activation process, J. Mater. Sci. 53 (2018) 13790–13800.

Chapter 4: -

Instruments and Apparatus

- **Sample Characterization techniques:**

The prepared Gel Polymer electrolyte was characterized to find out its electrochemical performance and the physiochemical properties. The electrochemical Performance was carried out by the different characterization technique such as Cyclic Voltammetry, Charge Discharge and Electrochemical Impedance Spectroscopy. The physiochemical characterization involves X-ray Diffraction (XRD) Scanning and Tunnelling electron Microscopy (SEM & TEM), Differential Scanning Calorimetry (DSC), Thermo-Gravimetric Analysis (TGA), Fourier Transform Infrared Spectroscopy (FTIR), electrical and electrochemical measurements etc.

- **Physiochemical Characterization:**

X-Ray Diffraction (XRD): XRD is a technique used to determine the crystallinity of polymers recognition of crystalline phases and its orientation. It is based on the constructive interference of the monochromatic X Rays and a crystalline sample. X rays are shorter wavelength (λ=0.154 nm) electromagnetic radiation that are generated when electrically charged particles with sufficient energy are decelerated. The X-rays generated are collimated and directed towards the sample where the interaction of the x rays and the incident rays produces a diffracted ray which is detected processed and counted. The intensity of the diffracted ray is scattered at different angles of the material are plotted to get a diffraction pattern.

XRD is used to study the properties of the formed polymer electrolytes XRD patterns of the polymer electrolytes was recorded at room temperature in an X-ray diffractometer using Cu-Ka radiation at an applied voltage of 40 kV and current of 40 mA with a scan rate of 0.3 degree/s over the range of 2 θ from 10-70 degree.

In the year 1895, the German physicist Roentgen discovered X-rays and so named due to the unknown nature at that time. These rays were invisible, traveled in straight lines and affected the photographic plate like ordinary light. Also, these rays show more penetrating power than light. In the year 1912, the exact nature of X-rays and diffraction phenomenon of x-rays by atomic planes of crystals were properly discovered. This discovery showed the wave nature of

X-rays and explored a new direction to investigate the structure of matter. Solid matter can be divided as follows:

- **Amorphous:** The atoms are arranged in a random way similar to the disorder we find in a liquid. Glasses are amorphous materials.

Crystalline: The atoms are arranged in a regular pattern, and one smallest volume element that by repetition in three dimensions describe the crystal. This smallest volume element is called a unit cell. The dimensions of the unit cell are described by three axes: a, b, c and the angles between them alpha (α), beta (β), gamma (γ). About 95% of all solids can be described as crystalline. X-rays are electromagnetic radiation of almost same nature as light but having

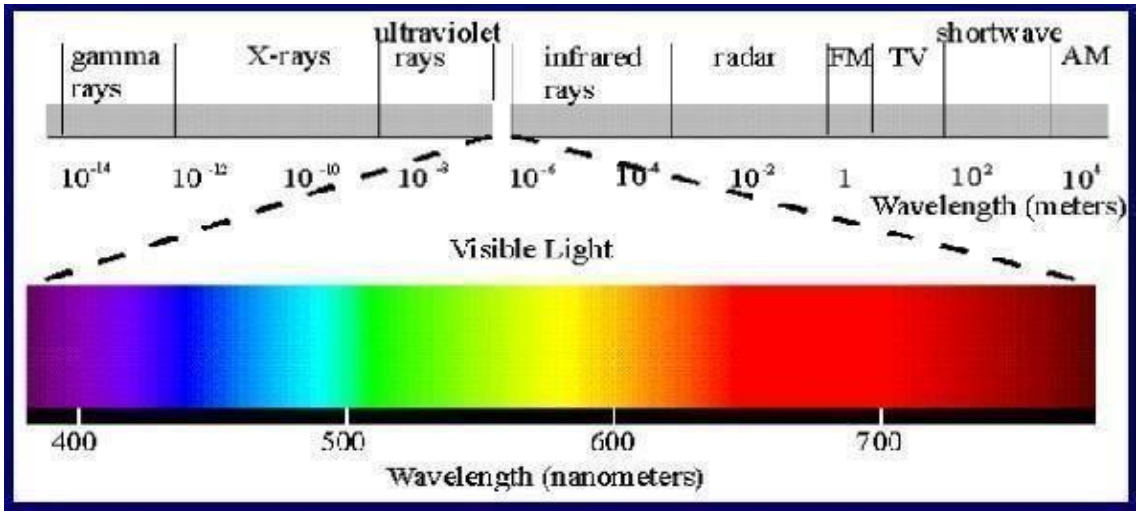


Fig 4.1: Illustration of electromagnetic spectrum

shorter wavelength of 0.5 to 2.5 Å regions. X-rays occupy the region between gamma and ultraviolet rays in the entire spectrum.X-rays are electromagnetic radiation of almost same nature as light but having shorter wavelength of 0.5 to 2.5 Å regions. X-rays occupy the region between gamma and ultraviolet rays in the entire spectrum.

Diffraction is a scattering phenomenon in which a large number of atoms participate and act as scattering centre. X-rays scattered by the atoms which are periodically arranged in the lattice, have definite phase relationship in between them. In some scattering direction, destructive interference takes place but, in few directions, constructive interference occurs and forms the diffracted beam. ***"A diffracted beam may be defined as a beam composed of a large number of scattered rays mutually reinforcing one another."***

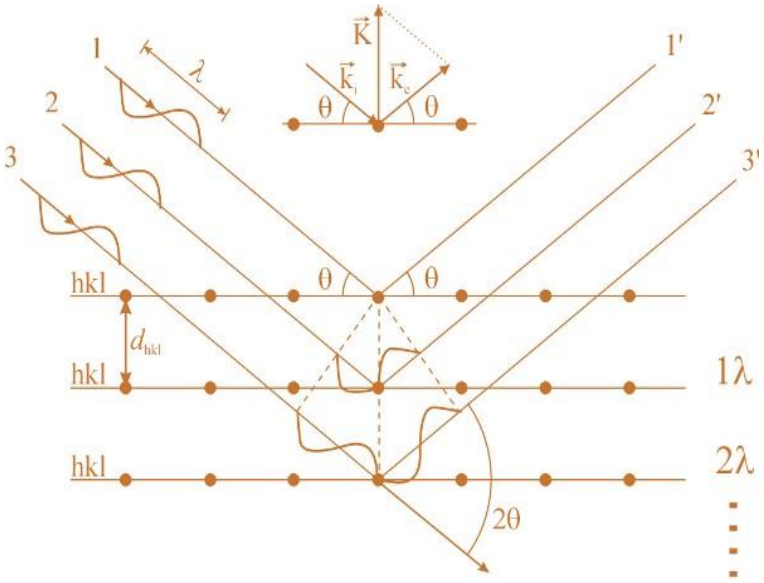


Fig 4.2 Visualization of Braggs Equation

Bragg's Law: The law states that when the X-Ray is incident on to a crystal surface its angle of incidence θ will reflect with the same angle of scattering θ. And when the path difference d becomes equal to a whole number n of a wavelength a constructive interference will occur. A set of crystallographic lattice planes is irradiated with X-rays impinging the surface of the lattice planes at an angle θ. The inter-planar spacing d_{hkl} sets the difference in the path length for the ray scattered from the top plane and the ray scattered from the bottom

plane. The difference in the path length is 2dSinθ. However constructive interference can only take place when the difference in path length is equal to λ.Thus Braggs equation was formed and can be written as :

$$\mathbf{2dSin\theta=n\lambda}$$

where n is the integer and θ is the angle of scattering and d is the interplanar distance.

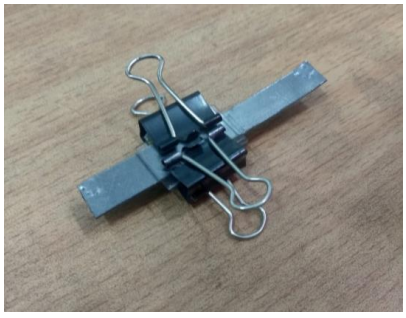


Fig.4.3 Photograph of EDL Capacitor containing gel polymer Electrolyte

The basic measurement geometry is depicted in Fig 2. The angle of both the incoming beam and exiting beam is θ with respect to the specimen surface. The diffraction pattern is collected by varying the incidence angle of the inward X-ray beam by θ and the scattering angle by 2θ while measuring the scattered intensity as a function of 2θ. Therefore, two angles must be varied during a θ/2θ scan in one case X-Ray source remains fixed while the sample is rotated around θ and the detector moves by 2θ. In another case the sample was fixed and both the source and detector were rotated by θ respectively but the sense of rotation was different. The central part of a diffractometer or goniometer performed the rotations. The sample was loaded on to the rotational axis while the detector and the x-ray source moves along the periphery but the axes coincide.

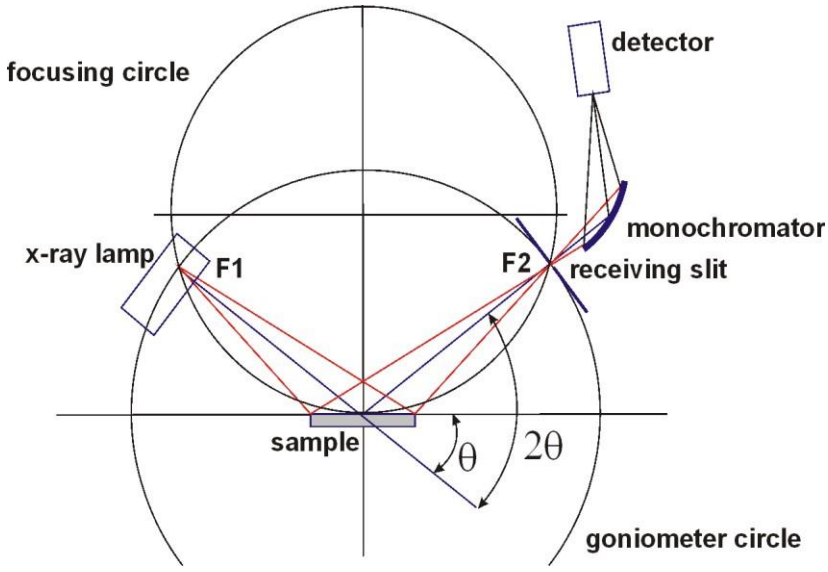


Fig 4.4 Schematic Representation of θ/2θ diffraction in Bragg-Brentano geometry



Fig4.5. XRD of Jadavpur University, Department of Physics (Bruker D8 Advance)

- **Scanning Electron Microscopy (SEM):**

Scanning electron microscopy is a popular technique to obtain high resolution image and detailing of the surface information of the samples The images formed have a greater resolution than light

microscopy A SEM projects a focussed stream of electrons over the surface of a sample and collects

the different signals produced using specialized detectors. The electrons in the beam interact with the atoms within the sample thus generating information about the surface topography and composition. A secondary electron detector and a Back Scattered electron detector are used for high resolution imaging in SEM. The unique configuration of the SEM will ultimately determine its resolution and imaging modes. A wide range of solid materials can be analysed using SEM. A Secondary Electron Detector (SED) and Back Scattered electron Detector (BSD) are the most commonly detectors used in SEM.

- **Working Principle of a Scanning Electron Microscope**:

Electrons are produced at the top of the column in an electron gun and the electrons are accelerated through the column by a vey high potential of (1 keV-30 keV). Condenser lenses and apertures act to reduce diameter of the beam. The final lens in the column is the objective lens which finally focuses the beam on the sample surface. The diameter of the beam in SEM ranges from 2 nm to 30 nm depending on the type of electron gun accelerating voltage and lens configuration. The sample

is mounted on the stage and a vacuum is maintained by a combination of the pumps. Some microscope allows for variable pumping allowing the sample chamber to be kept at a low vacuum. The scan beam directed towards the sample is controlled by scan coils situated above the objective lens. The scanned beam strikes the sample generating a variety of signals such as scattered electron and backscattered electron useful for characterization. These characteristic signals are detected by the detectors. These scan generators together with an external computer compiles the information from the scan generator with the intensity acquired by the detector allowing a grayscale image to be displayed and viewed in real time pixel by pixel. Magnification results from the size of the scanned area wherein higher magnification corresponds to smaller scanned areas.



Fig.4.6 FESEM of Jadavpur University, Department of Physics (Inspect F50)

Main Components of SEM:-

1. Electron Gun
2. Condenser Lenses
3. Objective Lenses
4. Detectors
5. Sample Stage
6. XY scan coils & scan generator
7. External Vacuum Pump

Electron Gun: It emits a bright and coherent stream of electrons that can be defocused onto the sample by lenses within the column. SEMs use three type of electron emitters tungsten filament solid state hexaboride crystals and field emission guns (FEG).

Scanning Coil: After the beam is focused, scanning coils are used to deflect the beam in X and Y axes so that it scans in a raster fashion over the surface of the sample The scanning coils are synced with the detector and the software in such a way that the image on the monitor

allows real time images to be viewed

Sample Chamber: Samples are mounted and placed into a chamber that is evacuated. The sample chamber can include a translational stage tilt and rotational devices electrical feed throughs to external devices temperature control for cryogenic cooling or heating optical cameras and to assist in analyzing the sample.

Detectors: When the electron beam interacts with a sample in SEM it leads to generation of different signals which need to be detected. In general, we need detectors to distinguish between secondary electrons backscattered electrons and characteristics X-rays. Depending upon the accelerating voltage the signal comes from different penetration depths.

Electron Lenses:

Electron beam can be focused by electrostatic or magnetic field. But electron beam controlled by magnetic field has smaller aberration, so only magnetic field is employed in SEM system. Coils of wire, known as "electromagnets" are used to produce magnetic field and the trajectories of the electrons can be adjusted by the current applied on these coils.

Condenser lens:

The electron beam will diverge after passing through the anode plate from the emission source. By using the condenser lens, the electron beam is converged and collimated into a relatively
parallel stream. A magnetic lens generally consists of two rotationally symmetric iron pole pieces in which there is a copper winding which provides magnetic field. There is a hole in the center of pole pieces that allows the electron beam to pass through. A lens-gap separates the two pole pieces, at which the magnetic field focuses the electron beam. The position of the focal point can be controlled by adjusting the condenser lens current.

Sample preparation:

As we mentioned earlier that FESEM is vacuum based instrument, so sample must be vacuum tolerant. In addition to that, strong radiation by electrons can damage or destroy a sample through heating or other effects. Even in quite good vacuum (10^{-8} mbar), samples can

become coated with gold/platinum in the microscope to retain the true surface details. Some samples, those are insulating in nature, are charged up under the electron beam and repel the incoming electron beam. This degrades the resolution and usually requires some prevention technique such as coating the sample with a conducting layer.

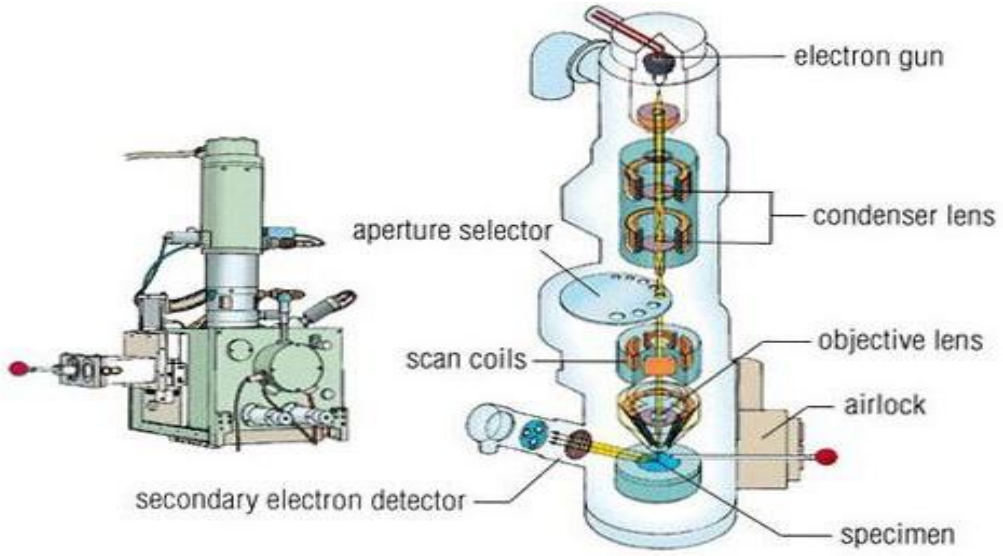


Fig 4.7 Schematic Drawing of a conventional Scanning Electron Microscope (SEM)

- ## Fourier Transform Infrared Spectroscopy (FTIR):

This technique is used to understand the vibration of molecules. Each and every molecule comprises of functional group which have a discrete vibrational energy used to identify the same. The electromagnetic spectrum consists of different regions corresponding to different values of Energy frequency and wavelength. The wavenumber is defined as the inverse relation between wavelength and frequency. When IR is transmitted through the sample if the frequency of bonding of the sample exactly matches with a particular frequency of the IR region and some peaks are observed due to resonance. Each of the peaks corresponds to a particular kind of vibration of atoms in the molecule. The basis of FTIR analysis is Beers Law which provides a relation between concentration to absorbance given by the following relation:

$$\mathbf{A = \mu \varepsilon c}$$

where A is absorbance $\boldsymbol{\mu}$ is the absorptivity, $\boldsymbol{\varepsilon}$ is the path length and c is the concentration.

When an interferogram is measured with a sample in infrared beam and Fourier transformed a single beam is produced. The transmittance is defined as:

$$T = I / I_0$$

where I and I_0 are the intensity of beam with and without sample respectively

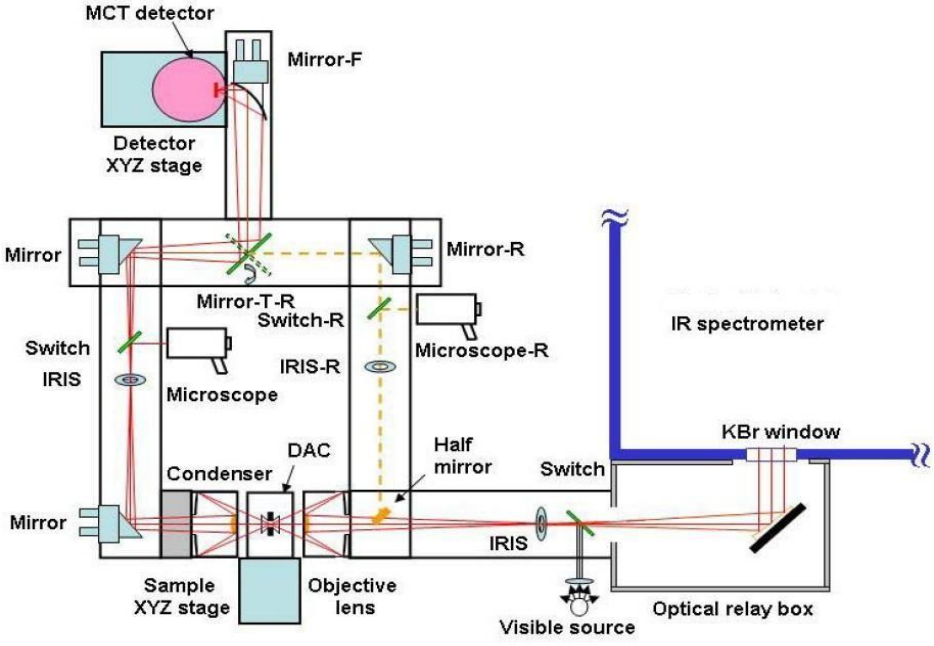


Fig 4.8. Schematic Diagram of FTIR Spectrometer

i.e. I_0 is background spectrum and I is sample spectrum. Absorption A can be obtained from taking logarithmic value of transmittance T as

$$A = - \log_{10} T$$

For qualitative study the IR spectra can be plotted in either transmittance and absorbance mode

Working Principle of FTIR:

The three major parts of an FTIR are the source, interferometer, and detector. The source is typically a broadband emitter such as a mid IR ceramic source (50-7,800 cm^{-1}), a near IR halogen source (2,200-2,500 cm^{-1}) or a far IR mercury lamp (10-700 cm^{-1}). The interferometer is the heart of FTIR and consists of a beam splitter a stationary mirror and a moving mirror and a timing laser. The beam splitter splits the light into two half one half goes towards the stationary

mirror whereas the other half reaches the moving mirror. The common beam splitters include KBr for mid IR range (375-12,000 cm^{-1}) Quartz for near IR (30-12,000 cm^{-1}) and Mylar for far IR The beams from the moving mirror gets recombined at the beam splitter and are redirected towards the sample. The difference in the path of the mirror causes constructive and

destructive interference over the course of time it takes for the moving mirror to pass. A laser with known

wavelength is taken to determine the position of the moving mirror. He-Ne lasers are the industry norm due to their excellent wavelength stability compared to solid state or diode laser.

- **Differential Scanning Calorimetry:**

Differential Scanning Calorimetry or DSC indicates the measure of change in heat flow to the experimental sample and the reference sample while they are subjected to a tempoerature control program. The heat capacity of sample is tracked as there is a change in heat flow. Thus it allows detection of different transitions such as glass transition melts phase change and curing. From thermodynamics it is well known that heat capacity from 0 K to the temperature of interest to study material properties.With known heat capacity of the sample and known heat transitions we can determine the thermodyamic properties of the sample.

Thermodynamic Equations :

1. Enthalpy:- $H=\int_0^T C_p dT$
2. Energy:- $U=\int_0^T C_v dT$
3. Entropy:- $S=\int_0^T \frac{C_p}{T} dT$ or $S=\int_0^T \frac{C_v}{T} dT$

4. Gibbs Free Energy:- G = H - TS
5. Helmothz Free Energy:- F=U – TS

Calorimetry is generally based on the following relationship:

dQ = C.ΔT = c. m. ΔT

In differential form assuming time independent sample mass and specific heat capacity

$$dQ = C.\Delta T = c.m.\Delta T$$

$$\frac{dQ}{dt} = \emptyset = C.\frac{dT}{dt} = c.m.\beta$$

In differential form assuming time independent sample mass and specific heat capacity where dQ is the heat exchanged ΔT is the temperature change caused by the heat exchange C is the heat capacity c=C/m is the specific heat capacity and m is the sample and β is the scan rate.

DSC operates in the temperature range of −80℃ to 500℃ in a nitrogenous atmosphere. In the case of semi-crystalline polymer matrix such as P(VdF-HFP) we can calculate X_c which is the percentage of crystalline phase of P(VdF-HFP) in the gel polymer electrolyte



`

Fig 4.9. DSC Instrument (TA Instrument model: Q 2000)

- **Working Principle of DSC:**

In the above shown image we have a DSC instrument which has been used. In the above figure we see that there is a robotic hand which is used to pick the aluminium pan where the sample is placed manually. The reference pan is also placed in the chamber.Both the reference pan and the aluminium pan were encapsulated using a lead. Now the isothermal heating and cooling actions are programmed in the computer. The heating scan rate is set to the value of 10℃/min in the software. The programm was set for cooling in the first phase where it was cooled from room temperature to -50℃ isothermally. In the next step the temperature control was set in such a way that the temperature first increases from -50℃ to room temperature and then from room temperature to 200℃. During this

process a constant flow of N_2 (50ml/min) is maintained. Now after the process is over the pans ware dropped in the space just outside the box.

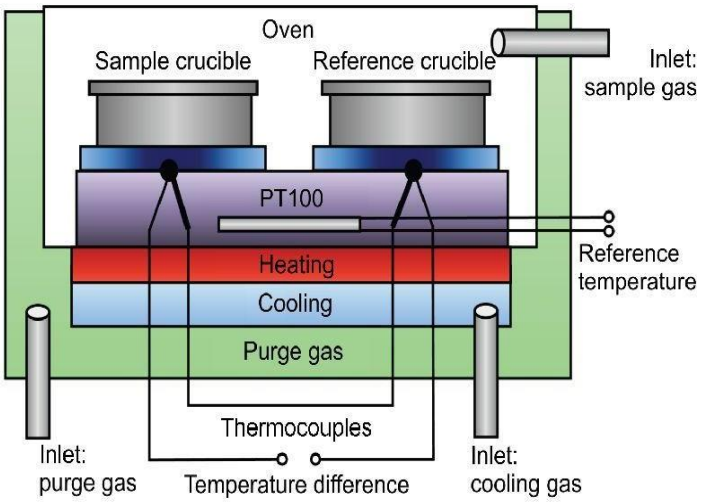


Fig 4.10. Schematic Diagram of DSC Measurement Technique

- **Thermogravimetry Analysis (TGA):**

Thermogravimetric Analysis or TGA measures change in the experimental material as a function of temperature under controlled nitrogenous atmosphere. The weight of the sample was first measured in an analytical balance that remains outside the furnace. The mass loss is observed in TGA as during any thermal event the loss of volatile component takes place. In chemical reactions such as combustion weight losses are involved whereas melting does not involve weight loss. The weight of the sample is plotted against temperature to demonstrate thermal transitions in the material such as loss of solvents and plasticizers in the Gel Polymer Electrolyte. It has widespread applications such as determination of carbon black content decomposition temperature performance of stabilizers low molecular weights of monomer in polymer.

Working Principle of TGA:

A TGA instrument (TA Instruments, Model SDT Q 600) was used to find the range of stabilization of the sample. The sample of weight 7-10 mg was taken in an empty alumina pan and balancing it against alumina in another pan. The temperature of the furnace was increased at a rate of 10 ℃/min in N_2 atmosphere. The change in the weight and heat difference was noted for information regarding thermal property.

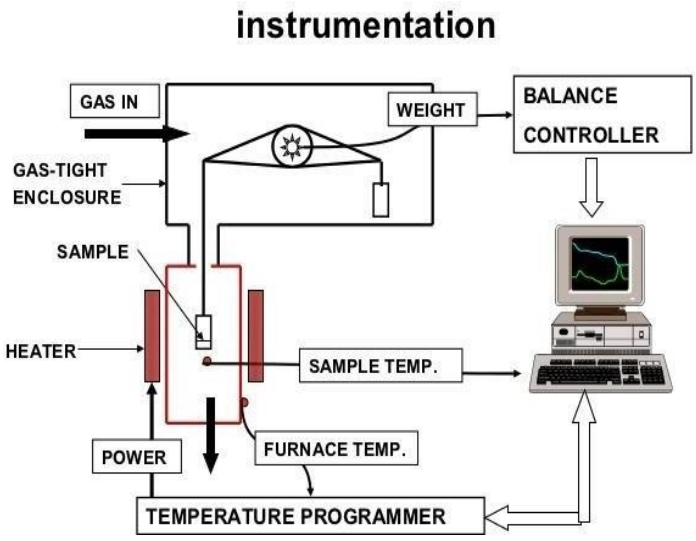


Fig 4.11. Schematic Diagram of Thermogravimetry Analyzer

Electrochemical Characterization of Sample:

To characterize the electrochemical properties of the EDLC or supercapacitor we have adopted different physical techniques such as Cyclic Voltammetry and galvanostatic charge discharge studies.

Cyclic Voltammetry:

The Cyclic Voltammetry is an important probe characterization technique where the potential is applied to the electrodes which is a function of time. The potential of the working electrode is swept between two set points at a constant scan rate. In CV the initial set point is chosen as such that no electrode reaction occurs that is it gives nearly zero current for the applied potential. The start and end points are the equilibrium positions or open circuit potentials. The nature of the current is observed as a function of the scanned potential. The reversal of the potential scan rate leads to an increase in the current because of the reaction of the products. In CV during the charging cycle the current value rises till it reaches the extreme set point and again decreases in the discharging cycle where the current becomes nearly zero. Thus, the forward and backward reaction takes place in the charging and discharging cycle at a fixed potential scan rate.

The cyclic voltammetry of an ideal capacitor having negligible internal resistance shows a perfect rectangular shape and it is scan rate dependent. For real capacitor the deviation from the rectangular shape is observed because it is a series combination of internal resistance, R

and capacitance C.

In our study all the Cyclic Voltammetry Measurements were taken with the help of Gamry Instruments (Interface 1000), and analysed using Origin Lab Software for different scan rates at a fixed voltage range from -1 V to 1 V. The value of the specific capacitance can be found using the expression:

$$C_{Sp}^{CV} = \frac{\int I\, dV}{2 \times m \times s \times \Delta V}$$

In the above expression $\int IdV$ is the integrated area of the CV curve, m is the single electrode mass of the active material in g, s is the scan rate and ΔV is the voltage range.

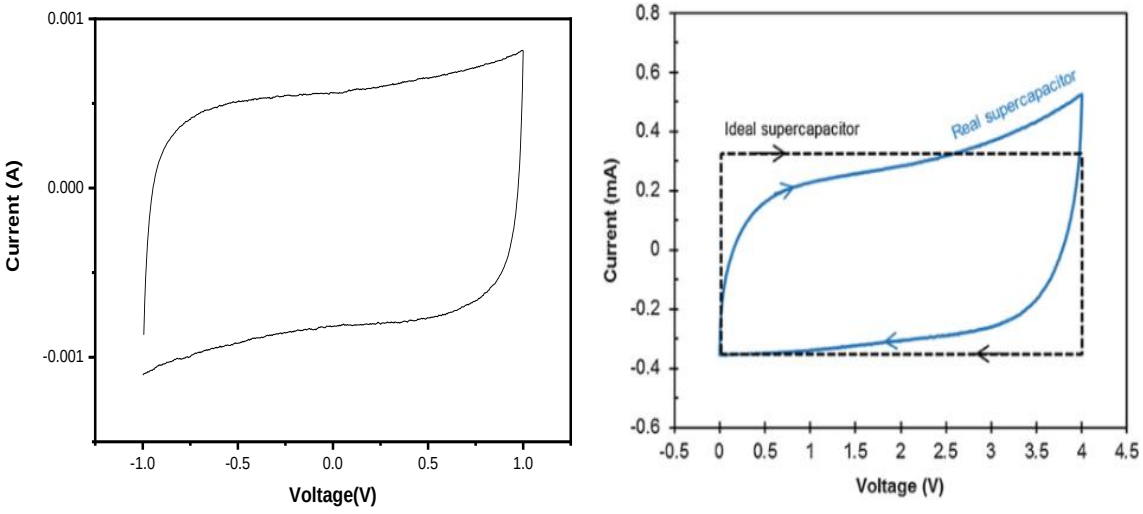


Fig. 4.12 Cyclic Voltammetry of a) real supercapacitor and b) ideal supercapacitor

Charge-Discharge Studies:

The information about an electrochemical system is generally gained by applying an electrical perturbation to the system and observing the changes in the characteristic behaviour of the system. In this case perturbation used is either a voltage step (potentiostatic method) or a current step (galvanostatic method). In case of charge discharge technique for characterization of a super capacitor it is necessary to consider the behaviour of real capacitor system represented by an ideal capacitance Cc connected in series with internal resistance R.

- Potentiostatic (Voltage Step Method): When a potential step is applied across a capacitor cell the capacitor charges and an exponentially decaying current is observed. The behaviour of the current I with respect to time on application of potential step V_o can be expressed as:

$$I = \frac{V_o}{R} \exp\left(-\frac{t}{\tau}\right)$$

where τ=RC is the time constant. The capacitor cell starts discharging when the operation is reversed and the pattern is like the discharge curve with reverse polarity. The charge discharge

curves can be integrated to obtain the total charge stored or released. The capacitance C can be calculated as the total charge divided by the total applied voltage V_o.

- Galvanostatic (Current step) Method: When a supercapacitor cell is charged by a constant current i, the total voltage V developed across the cell can be expressed as:

$$V = iR + \frac{\int I\, dt}{C}$$

As the current is constant the expression can be written as :

$$V = i\left(R + \frac{t}{C_c}\right)$$

For a current step the voltage across an ideal supercapacitor cell whose capacitance value is increased linearly with time. After full charging of the supercapacitor at the maximum permissible or desired voltage level it is discharged galvanostatically. The decrease in the voltage with respect to time is almost linear. The decrease in voltage across the cell is also linear with respect to time. In the real EDL supercapacitor a sharp drop is observed while charging discharging. An ohmic internal resistance is referred to as equivalent series resistance of the supercapacitor cell. ESR is calculated using the following relation:

$$ESR = \frac{\Delta V_r}{2 \times i}$$

Here ΔV_r is the internal ohmic voltage drop, and i is the applied discharge current. The overall capacitance of the supercapacitor cell have been calculated from the linear portion of the discharge curve using the relation: $C_{cell}^{dis} = \frac{i}{m_{tam} \times \frac{\Delta V}{\Delta T}}$, where i is the discharge current m_{tam} is the total active mass in g and $\Delta V/\Delta t$ is the slope of the discharge characteristics after IR drop. In, symmetrical cell system, the specific capacitance referred to a single electrode (C_{sp}^{dis}) is related to overall capacitance of the cell (C_{cell}^{dis}) by the following relation:

$C_{sp}^{dis} = 4 \times C_{cell}^{dis}$. The charge-discharge experiment can be carried out for several cycles (from 4000 to 8000 cycles) to test the stability cyclic efficiency of the cell. The charge-discharge experiment was performed by measuring the voltage as a function of time at constant currents in the range 0.5 – 5.0 mA. The ratio of discharge time to charging time referred to Coulombic

Efficiency (CE), is calculated using following relation:

$$\eta\% = \frac{\Delta t_d}{\Delta t_c} \times 100\ \%$$

where , Δt_d and Δt_c are discharging and charging time obtained from charge and discharge curve respectively.

The energy density and power density are calculated from the charge discharge characteristics at different current rates using the following relations:

$$E = \frac{C_{cell}^{dis} \times (\Delta V)^2}{2} \times \frac{1000}{3600}$$

and

$$P = \frac{E \times 3600}{\Delta t}$$

Where C_{sp}^{dis} is the specific capacitance and ΔV is the cell voltage and Δt is the discharge time.

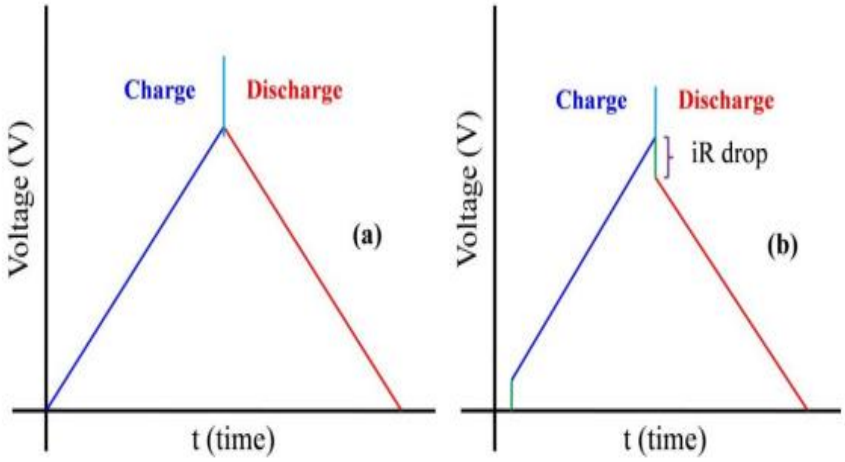


Fig. 4.13 Charge discharge behaviour of a) an ideal supercapacitor and b) EDL capacitor

- **Electrochemical Impedance Spectroscopy:**

Electrochemical impedance spectroscopy is a very effective method to study in-depth the electrochemical performance of electrical double layer (EDL) capacitors. Electrochemical impedance spectroscopy works by applying a small alternating current (ac) potential over a wide range of frequencies to an electrochemical sample and the resulting changes in current is measured which is caused by the electrochemical impedance of the experimental sample as a function of frequency. Nyquist plot shows the connection of imaginary impedance function (Z″) to real

impedance function (Z′) and correlates with the system stability. The impedance pattern of an ideal capacitor shows a steep rising dispersion line overlapping with imaginary axis of the impedance plot which implies a straight line parallel to the y axis. The impedance pattern of a real capacitor shows a semicircle. The equivalent series resistance (ESR) value of the electrical double layer (EDL) capacitor observed at high frequencies is obtained from the intercept of the Nyquist plots with the

real impedance spectra axis which is defined by R_1. ESR value is mainly determined by the electrolyte resistance and contact

resistance of the active material or current collector interface. The next intercept in real impedance axis which is defined by R_2 indicating the charge transfer resistance (R_{ct}) which is calculated by the difference between two intercepts ($R_{ct} = R_2 - R_1$). The value of the R_{ct} is also defined as the diameter of the semicircle portion of the Nyquist plot in the high frequency range, which is dominantly affected by the electron transfer process in electrochemical sample system. The inclined line suggests ion diffusion behaviour of the electrolyte inside the composite electrode at intermediate frequencies. The almost straight tail is mainly affected by diffusion process which is observed in lower frequencies region.

The EIS measurements are done using the Gamry instrument. The frequency range expands from low frequency range of 10 mHz to 1 MHz The overall capacitance can be measured from the relationship:

$$C_{overall}^{EIS} = -\frac{1}{2 \times \pi \times f \times Z''}$$

Where f is the frequency in Hz and Z'' is the imaginary part of the total impedance measured. The values of specific capacitance were determined by multiplying the overall cell capacitance by a factor of two and divided by the mass of a single electrode active material in g.

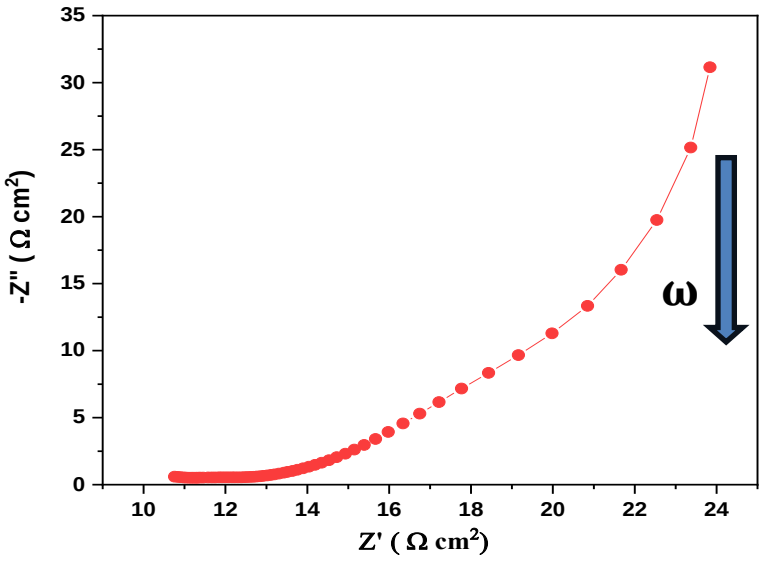


Fig 4.14. Impedance plot of a real supercapacitor

Full Cell Lithium-Ion Batteries:

Full cell LIBs consists of the cathode, anode, and polymer electrolyte. A schematic diagram of a coin cell type full cell LIB can be shown in Fig. 2.19. Here, CR2032 coin cell type LIBs has been used. The sizes of the different kinds of coin cells restrict the diameter of the electrode material that can be used, for example, CR2032 is 20 mm in diameter; the electrodes are usually 13 mm. LiCoO2 and LiFePO4 have been used as an active material of cathode while graphite has been used as an active material of anode. The electrochemical characteristics of a rechargeable lithium battery are generally tested using charge-discharge and cycling. The charge-discharge cycles of Li ion batteries are obtained through a galvanostatic method, in which current is controlled (i.e. kept constant) and the potential is determined as a function of time. Since the variation of potential in electrochemical system is determined as a function of time, the technique is also called as chronopotentiometry. For the working electrode a negative current would cause reduction and a positive current, oxidation. The potential of electrochemical cell varies according to Ohm's law with the applied current. The input and resultant output profile of the constant current experiment is shown in Fig 4.15.

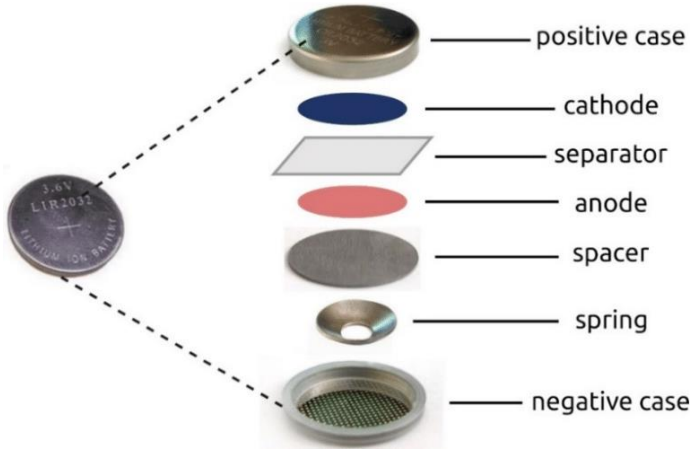


Fig 4.16. A schematic diagram of different components of Coin cell battery

The electrochemical redox reaction takes place at the electrode-polymer electrolyte interface when the current passes through the cell. The galvanostatic charge-discharge experiment is used for measuring the specific capacity and rate capability of the material. The charge and discharge rate is selected depending upon the theoretical specific capacity of the cathode material under study. The current used for charging discharging of the electrochemical cell under study is indicated by C rate. The theoretical capacity of the electrode (cathode) and expressed as CED = WAM×C. Here, WAM is weight of the active material and C is the theoretical specific capacity of active material. The theoretical capacity of

LiCoO2 and LiFePO4 active cathode materials are 160 and 170 mAh/g respectively [8-9].The C-rate, which is the current rate at which charge discharge cycling is performed, can be deducted as follows AM rate W C C n × = (2.33) , where, Crate is the rated capacity i.e total capacity of the battery could deliver in n hours. The coin cell CR2032 type lithium-ion full cell is fabricated inside the argon gas filled glove box (mBRAUN, LAB star ECO) with H2O < 0.5 ppm O2 < 0.5 ppm. The electrochemical performances of the cells assembled as above are studied using VMP3 (Biologic) multi-channel potentiostat/ Galvanostat and analyzed using EC Lab® software at room temperature (25 °C ± 5).

- **Li+ ion transference number measurement technique:**

Transference number is defined as the ratio of conductivity of a specific ion to the total conductivity. In ion conducting polymer electrolytes have more than one conducting ions such as cations and anions both contributing significantly to the total ionic conductivity. It is essential to know the contribution of cationic and anionic to the overall conductivity. The

cationic and anionic transference number can be expressed by the following relation: $t_+ = \frac{\Sigma I_+}{\Sigma(I_+ + I_-)}$, and $t_- = \frac{\Sigma I_-}{\Sigma(I_+ + I_-)}$ where $\sum(I_+ + I_-)$ is the total current expressed as the sum of the partial current due to the mobile cations and anions present in the electrolyte. Therefore, Li^+ ion transference number in lithium polymer electrolytes is a crucial issue due to their application in solid-state lithium-ion battery (LIB) as both the electrolyte and the separator. There are various experimental techniques to measure the transference number such as (a) Tubandt's method, (b) Wagner's polarization technique, (c) Electrochemical potential measurement technique, (d) AC impedance technique, (e) DC conductivity method and (f) Combined DC/AC technique. 100 Bibliography In the present work, the Li+ ion transference number was measured using combined DC/AC technique proposed by Vincent and Bruce. According to this technique AC impedance of the cell was recorded having a symmetric cell configuration of M (Li metal) || MX (lithium polymer electrolytes) || M (Li metal) and charge transfer resistance was determined. Thereafter, the symmetric cell is polarized by applying a small DC polarization voltage (10 mV). The Li+ ion transference number was calculated by the following relation, $t_{Li^+} = \frac{[I_{ss}(\Delta V - I_0 R_0)]}{[I_0(\Delta V - I_{ss} R_{ss})]}$,where I_0 and I_{ss} are the initial and steady-state current respectively, ΔV is the polarization voltage, R_0 and R_{ss} are the charge transfer resistances measured before and after the DC polarization respectively. The frequency range of the impedance spectra was 100 mHz - 1 MHz.

Bibliography

[1] R. Reichelt, Editor, Scanning Electron Microscopy, Springer, New York, USA (2007).

[2] R. F. Egerton, Physical Principles of Electron Microscopy Springer, New York, USA (2005).

[3] G. Höhne, W. Hemminger and H. J. Flammersheim, Differential scanning calorimetry, 2nd edition (Springer) (2003).

[4] B. Wunderlich, Thermal analysis, Academic Press, New York (1990). [5] P. J. Haines, Thermal methods of analysis: principles, applications and problems, Blackie Academic& Professionals, London (1995).

[6] G. Schaumburg, Dielectric Newletter 1 ((March 1994)), p. 4.

[7] T. a. A. EC-Lab® Software, V10.1x, Biologic-Science Instruments, copyright Feb. 2011, EC-Lab® Software,Technique and Application, V10.1x, BiologicScience Instruments, copyright Feb. 2011.

[8] K. Karuppasamy, P. A. Reddy, G. Srinivas, A. Tewari, R. Sharma, X. S. Shajan and D. Gupta, J. Membr. Sci. 514 (2016), p. 350.

[9] S. Ferrari, E. Quartarone, P. Mustarelli, A. Magistris, M. Fagnoni, S. Protti, C. Gerbaldi and A. Spinella, Journal of Power Sources 195 (2010), p. 559.

[10] J. Evans, C. A. Vincent and P. G. Bruce, Polymer 28 (1987), p. 2324

Chapter 5:

Characterization of Gel Polymer Electrolytes (GPE) and Results

- **Ionic Conductivity**

The ionic conductivity of gel polymer electrolytes (GPEs), a crucial parameter for designing electrochemical capacitors, is derived from the AC conductivity spectra. In Fig.5.1 , the AC conductivity spectra of BMIMTFSI based gel polymer electrolyte are depicted over a range of temperatures from 4 Hz to 8 MHz. These spectra reveal three distinct regimes: (i) the electrode polarization regime at low frequencies, dependent on electrolyte thickness, electrode material, and electrode-electrolyte interface, (ii) a frequency-independent regime in the mid-frequency range, representing ionic conductivity σ_{dc} and indicating long-range diffusion of charge carriers via hopping between favourable sites, and (iii) the ionic relaxation regime at high frequencies coupled with polymer chain dynamics.The AC conductivity can be effectively analysed using the universal power-law formalism proposed by Jonscher and modified by Almost-West. The Almond-West model expresses conductivity as:

$$\sigma(\omega) = \sigma_{dc} \times [1 + (\frac{\omega}{\omega_H})^n]$$

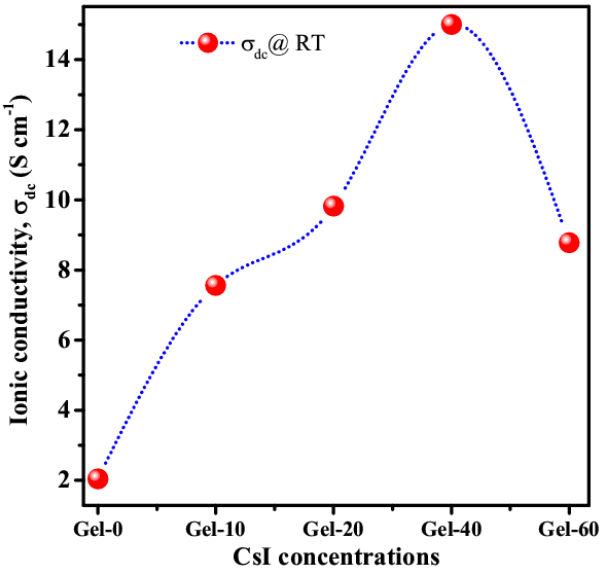


Fig.5.1 Ionic Conductivity of GPE for various samples

where σ_{dc} is the ionic conductivity ω_H is the hopping frequency of ions, and n is the power-law exponent (0 < n<1)

Fig. 2(b) displays the reciprocal temperature dependence of the ionic conductivity σ_{dc} obtained from AC conductivity analysis for all gel polymer electrolytes. These plots exhibit Vogel-Tammann-Fulcher (VTF) behaviour, as described by the following relation:

Where σ_0 is the pre-exponential constant, k_B is the Boltzmann constant, E_σ is the pseudo-activation energy related to the critical free volume for ion transport, and T_0 is the equilibrium Vogel scaling temperature on the absolute temperature scale. The ionic conductivity for GPEs

is fitted to using nonlinear least square fits, indicating strong coupling between the charge carrier dynamics and the segmental dynamics of the polymer chain.

Ionic Conductivity σ_{dc} is calculated and we can say that after preparation of gel polymer electrolyte of different concentration of CsI that the ionic conductivity in Gel Polymer Electrolyte with 40 mg concentration of CsI shows highest ionic conductivity when calculated from the VTF equation.

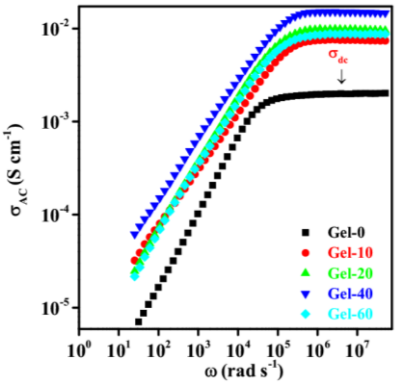


Fig. 5.2. AC conductivity Spectra at different room temperature

The conductivity of GPEs was measured using an LCR meter (HIOKI, model IM 3536LCR) in the wide frequency range of 4Hz–8MHz in the temperature range from 203 to 333K with 5K sweep cell in a cryostat with temperature stability of ±0.10K in vacuum (0.01mbar). The GPEs with thickness 0.4–0.5mm were sandwiched between two stain less steel (SS) blocking electrodes with diameter of about 10mm.From the ac conductivity spectra we can find that the Gel prepared with 40mg concentration of CsI has the optimised DC conductivity which is signified by the plateau. Thus highest ionic conductivity found for CsI with 40mg thus we can do a comparative study of the GPE IL and GPE CsI 40mg at different temperature values since we know that the EDLC device fabricated gets heated up when operated so we need to study the ionic conductivity patterns with varying temperature.

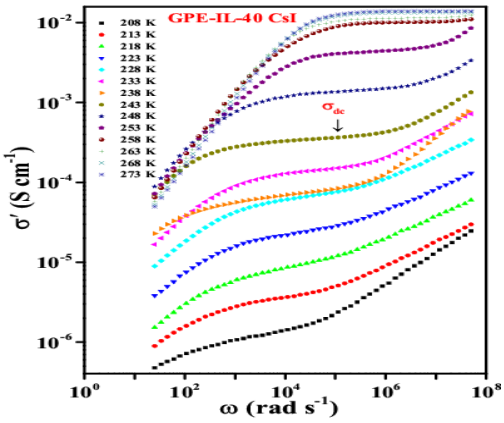


Fig.5.3. AC conductivity Spectra at different temperature

The DC conductivity (σ_{dc}) as we can see from the figure below increases with the increase in temperature but then we see a sharp fall due to the crystallization temperature (T_c) of ADN which is the plasticizer that we have used about which we have further studied in DSC

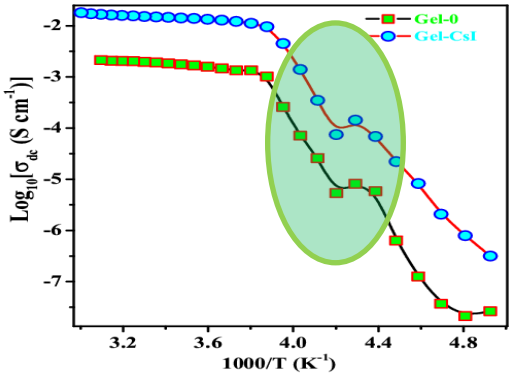


Fig.5.4. DC conductivity vs Temperature

Physiochemical Properties of Gel Polymer Electrolyte

- ### XRD Analysis

Initially, X-ray diffraction (XRD) analysis was employed to examine the phase structure of both the host polymer matrix P(VdF-HFP) and the gel polymer electrolytes doped with ionic liquid and plasticizers. In Fig. 5.5, the XRD patterns of the host polymer P(VdF-HFP) film, along with GPE IL,GPE CsI, GPE RbI, GPE KI are depicted. The XRD pattern of the host polymer P(VdF-HFP) displays distinct peaks at approximately $2\theta \approx 18.5°$, 20.2°, 26.8°, and 39.3°, corresponding to the (100), (110), (022), and (211) reflections of crystalline planes,

respectively. The copolymer P(VdF-HFP) exhibits a semi-crystalline phase overall. Notably, upon the addition of ionic liquid into the P(VdF-HFP) polymer matrix, significant alterations in the structural properties of the gel polymer electrolytes are observed. Several crystalline peaks have shifted, and the peaks around 2θ≈18.5° and 20.2° appear less intense and broadened. This outcome indicates a reduction in the crystalline phase of the gel polymer electrolytes following the introduction of ionic liquids and plasticizers.

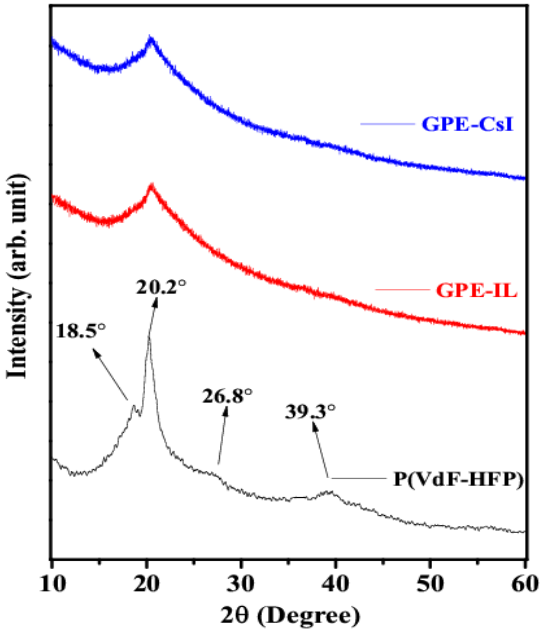


Fig 5.5 XRD patterns of the synthesized GPEs and P(VdF-HFP)

XRD patterns of (PVdF-HFP) film and GPEs were performed at room temperature using D8Bruker Advance AXS instrument using Cu-Kα radiation (λ=0.154 nm) with a scan rate of 0.2 ° s^{-1} and a step size of 0.02° over the angular range of 2θ ~ 10 °C-70 °C.

- **Differential Scanning Calorimetry (DSC):**

We utilized differential scanning calorimetry (DSC) to ascertain the fraction of the amorphous phase, a critical parameter influencing ion transport in gel polymer electrolytes. In Fig. , the DSC traces of both the pure host polymer P(VdF-HFP) film and gel polymer electrolytes embedded with different ionic liquids are presented. A distinct endothermic peak is observed at approximately 155°C, corresponding to the melting of the pure host polymer P(VdF-HFP) film. Following the blending of the ionic liquid with the host polymer matrix, the melting peak shifts towards lower temperatures, displaying a more asymmetrical shape, and the peak area is notably reduced. This shift indicates an increase in the fraction of the amorphous phase in the overall material due to the presence of a large proportion of ionic liquid in the polymer matrix. The degree of crystalline fraction (Xc) is calculated using the formula:

$$X_c = \frac{\Delta H_m}{\Delta H_m^0}$$

where $\Delta H_m^{\circ} \sim 104.7\ Jg^{-1}$ represents the melting enthalpy for 100% crystalline P(VdF-HFP) polymer matrix, and ΔH_m is the melting enthalpy of ionic liquid doped gel electrolytes, calculated from the area under the melting peak in the DSC traces. The values of T_m, ΔH_m, and

X_c for both pure P(VdF-HFP) film and gel polymer electrolytes are summarized. It is observed that both the melting temperature Tm

Sample Name	$T_{m(polymer)}$ (°C)	ΔH_m^0 (J g^{-1})	ΔH (J g^{-1})	X_c (%)
GPE IL	106.03	104.7	8.826	8.43
GPE CsI	11.68	104.7	6.56	6.26

Table 5.1 DSC Traces at Room temperature of samples

and melting enthalpy ΔH_m decrease with the introduction of ionic liquids. Additionally, the values of X_c decreases indicating an increase in the amorphous content of the polymer electrolytes due to the plasticization effect of ADN present in the GPE. Ionic liquids with larger cationic size and higher viscosity exhibit less penetration into the crystalline region of the P(VdF-HFP) polymer matrix, resulting in a weaker plasticization effect. The enhancement of the amorphous content renders the gel polymer electrolytes more flexible. Additionally, a distinct endothermic peak around ∼36.0°C and an exothermic peak around ∼7.0°C are observed. The crystallization temperature of ADN is observed to be -38 °C and the melting temperature of the ADN is obtained as -4 °C. The film or the polymer decomposes at the temperature of 130 °C.The values of crystallinity for GPE IL is 8.43% and the values of crystallinity for GPE with CsI taken as redox additive of 40mg weight is 6.26%

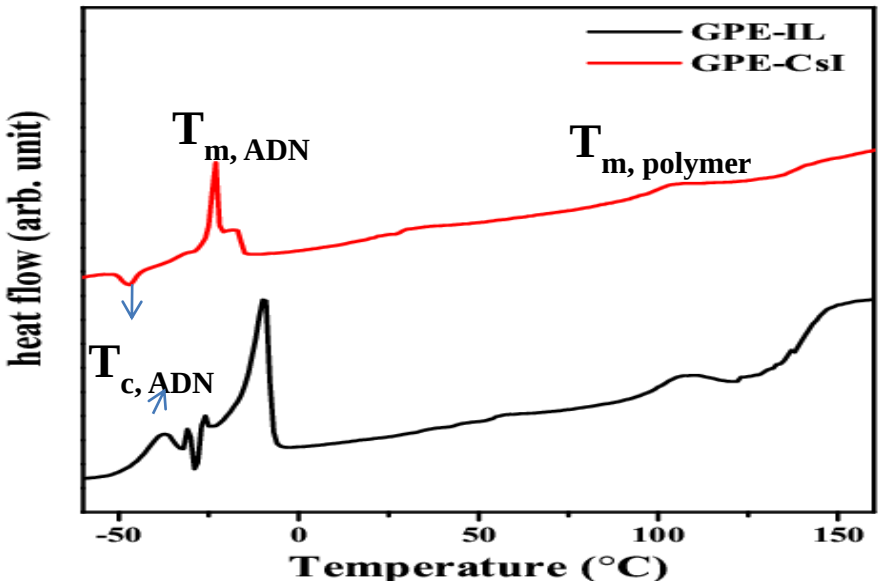


Fig.5.6 DSC traces of P(VdF-HFP) and synthesized GPEs

- **Thermo-Gravimetric Analysis (TGA):**

The thermal stability of both the pure P(VdF-HFP) polymer matrix and the gel polymer electrolytes doped with ILs is assessed through thermogravimetric analysis (TGA), as depicted in Fig. 5.7. It is

evident from Fig. 5.7 that the P(VdF-HFP) film exhibits minimal weight loss, indicating thermal stability up to approximately ~420°C. However, the thermal stability of the gel polymer electrolytes is notably diminished following the incorporation of ILs into the polymer matrix due to the decomposition of ionic liquids. The decomposition temperatures (Td) of Ionic Liquid BMIMTFSI can be seen as 330 ̊C. Nevertheless, all gel electrolytes demonstrate sufficient thermal stability for high-temperature applications.

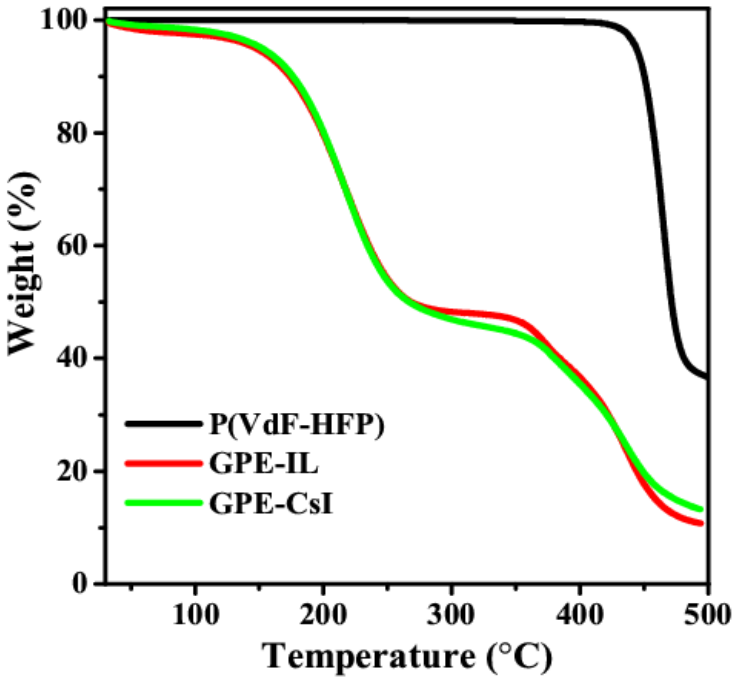


Fig 5.7 TGA traces of P(VdF-HFP) and synthesized GPEs

TGA experiments are conducted using instrument Q600 TA instrument already discussed in the previous chapter. The experiments are conducted from room temperature and the temperature is increased to 600 ℃ at a heating rate of 10 ℃/min.

- **Study of Morphology using Field Emission Scanning Electron Microscope (FESEM):**

SEM: From FESEM data we can conclude the Gel Polymer electrolyte with no redox additive or salt shows spherulite like micro-structures are observed in the SEM image

For the Gel Polymer electrolytes with redox additive, we can see the interconnected granules of the polymer with almost smooth surface. We also observe porous structures. It is observed that the spherulite structures of GPE IL slowly gets an irregular shape for samples having redox additive ie. CsI. Thus in Fig. 5.8 c) and d) we obtain irregular surface morphology.

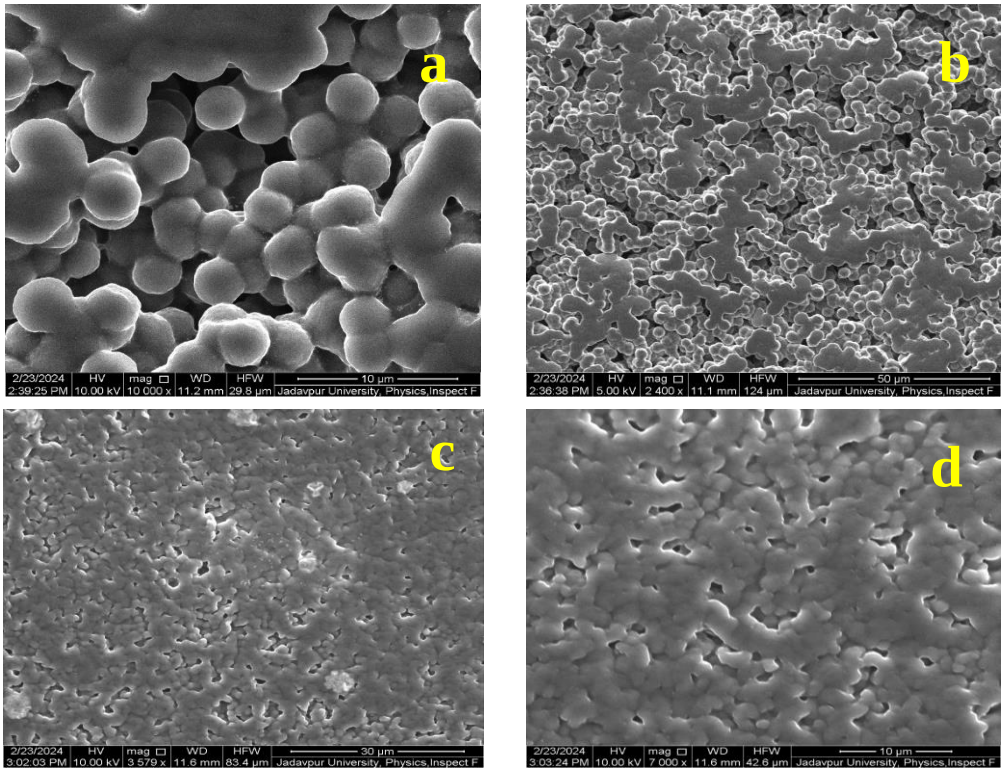


Fig 5.8 SEM image of a)GPE IL at a resolution of 10µm b) GPE IL at a resolution of 50µm c)GPE CsI at a resolution of 30µm and c)GPE CsI at a resolution of 10µm

- **Fourier Transform Infrared Spectroscopy (FTIR):**

TheFTIRspectraofdifferentGPEsarepresentedinFigure3a in the wavenumber range 750−4000 cm^{-1} to investigate the various possibilities of interactions. Figure 5.9 presents the FTIR spectra in the wavenumber range 700−1600 cm^{-1}. It is observed that the pure P(VdF-HFP) exhibits IR bands at 762, 796, and 976 cm corresponding to CH_2 rocking and C−F stretching, and CF_3 stretching

respectively. These three bands represent the crystalline α-phase of the P(VdF-HFP) polymer matrix. In addition, the pure P(VDF-HFP) shows peaks at 837 and 881 cm^{-1} , which correspond to CH_2 rocking and mixed mode and CF_2 and C−C symmetric stretching, respectively, due to amorphous β-phase of P(VDF-HFP). The ADN plasticizer based (GPE) polymer electrolyte shows different IR

bands at wavenumbers such as 773, 837, 881, 974, 1070, 1180, 1215, 1334, 1424, 2248, 2868, and 2947 cm^{-1} 881 cm^{-1}. The peaks at 837 and signify the existence of the amorphous phase in the

GPE

due to the interaction of the plasticizer with the polymer matrix. The GPE system shows that the peak intensity of the amorphous phase (881 cm^{-1}) increases, and the peak for crystalline phases (773 cm^{-1}) disappears. The peaks at 2248, 2868, and 2947 cm^{-1} arise from the addition of the plasticizer.

The peaks at 2868 and 2947 cm^{-1} correspond to the C−H stretching vibration band of the GPE.

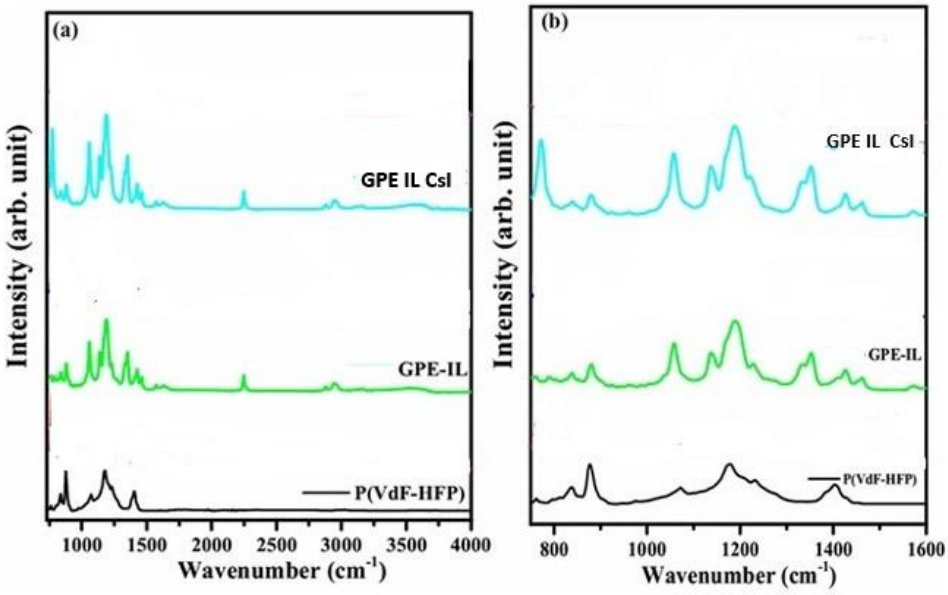


Fig. 5.9. FTIR spectra of P(VdF-HFP) and GPEs in the range of (a) 750-4000 cm^{-1} and enlarged view of the spectra in the range of (b) 750-1500 cm^{-1}

- **Electrochemical Potential Stability Window (EPSW):**

The electrochemical potential stability window (EPSW) of an electrolyte is a crucial factor in designing energy storage devices, as it directly impacts their performance. To determine EPSW, the Linear Sweep Voltammetry (LSV) technique was employed with a cell setup of SS|| GPEs||Ag, where SS and Ag denote stainless steel and silver metal plates, respectively. SS served as the

working electrode, while Ag functioned as the counter and/or reference electrode. In this setup, the EPSW of GPE-IL was measured to be around 5.68 V, with a cathodic stability (SS) of approximately -2.9 V and an anodic stability of around 2.78 V (as illustrated in Figure 5.10).

Introducing CsI redox active GPE (GPE-IL-DPA) resulted in a slightly lower EPSW of about 6.23 V, with cathodic and anodic stability values of approximately -3.0 V and 3.23 V, respectively. On the other hand, utilizing CsI-based redox active GPE (GPE-IL+CsI) extended the EPSW to around

6.23 V, with cathodic and anodic stability values of approximately -3.0 V and 3.23 V, respectively. Incorporating redox active GPE (GPE-IL + CsI) led to a modest enhancement in EPSW to approximately 6.23 from 5.86 V.Nevertheless, the redox additive used effectively maintained the EPSW above 6.0 V by stabilizing the ionic species. Consequently, this redox active GPE exhibits a wide EPSW range, rendering it suitable for supercapacitor (SC) applications.

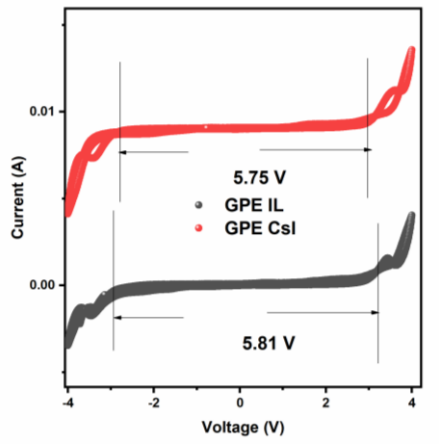


Fig 5.10. Electrochemical Potential Stability window

Electrochemical Properties of Gel Polymer Electrolyte

We have successfully developed solid-state EDL capacitors utilizing gel polymer electrolytes possessing favorable physicochemical characteristics. These properties include excellent thermal stability, high ionic conductivity at room temperature, and an expansive working potential window. These attributes directly impact the specific capacitance and energy density of the devices. We thoroughly examined the electrochemical performance of these EDL capacitors to assess their efficiency. We have done all our CV GCD and EIS measurements with the help of Gamry Instrument (Interface 1000).



Fig.5.11. Gamry Instruments used for CV, GCD and EIS Measurements

Cyclic Voltammetry (CV):

The cyclic voltammetry (CV) curve of Cell 1, constructed with GPE-IL electrolyte (Figure 5.12a), displays an almost rectangular shape within the voltage range of -1.0 to +1.0 V across various scan rates. This rectangular shape signifies the electrostatic (non-Faradaic) double-layer charge storage mechanism, indicating charge adsorption and desorption at the electrode-electrolyte interface. The area of the rectangle expands with increasing scan rate due to the accumulation of charge, which is contingent upon the electrode voltage.

In contrast, the CV pattern of Cell 2 (Figure 5.12b) at different scan rates reveals distinct Faradaic redox peaks. For comparative analysis the CV curves of various cells at a common scan rate are depicted in Fig. 5.12(c). Cell GPE CsI demonstrates two discernible redox peaks at -0.65 V and 0.74 V, respectively. These redox peaks stem from the irreversible redox reaction of iodide species derived from CsI. The dissociation of redox additives at the oxidation/reduction potential enhances charge species, thereby augmenting the area of the CV curve.

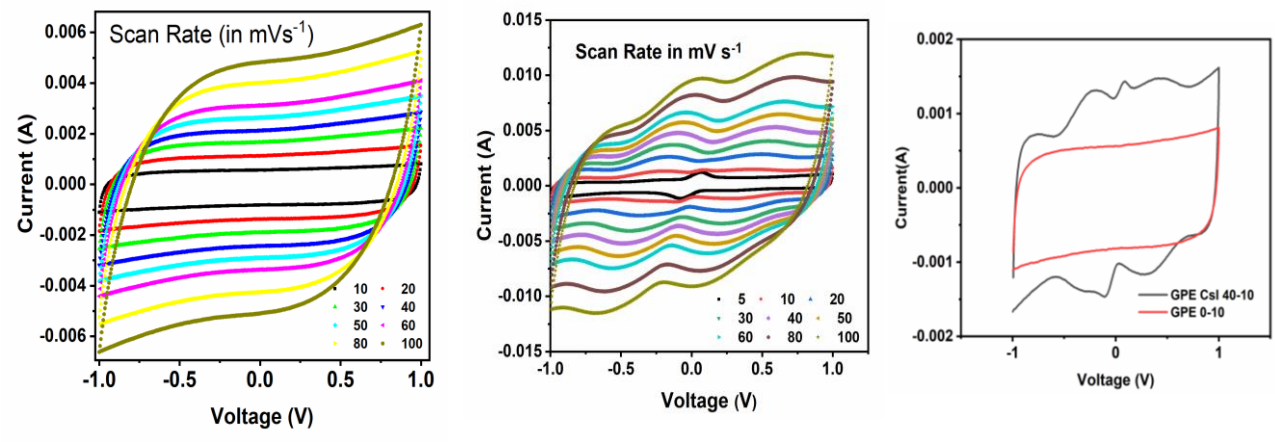


Fig.5.12. (L-R) (a) CV Curve for GPE IL at different scan rates, **(b)** CV Curve for GPE CsI at different scan rates and **(c)** CV curve for GPE CsI and GPE IL at common scan rate (10 mV/s)

The initial ion concentration influences the specific capacitance, which can be computed from the CV curve using the following relation:

$$C_{sp} = \frac{\int IdV}{s.m.\Delta V}$$

Here, $\int IdV$ represents the area under the CV curve, s is the scan rate, m is the mass of the active material for a single electrode, and ΔV is the potential window of the cell. GPE CsI exhibits the highest specific capacitance of 56.74 F/g at a scan rate of 10 mV s^{-1} owing to the presence of redox additives whereas GPE IL exhibits lower specific Capacitance of 34.27 F/g. However, as the scan rate increases, the specific capacitance diminishes due to a decrease in the rate of ion absorption or desorption through the porous carbon electrode. Additionally, at higher scan rates, the specific capacitance experiences a decline because of electrodeposition within the redox additive GPE.

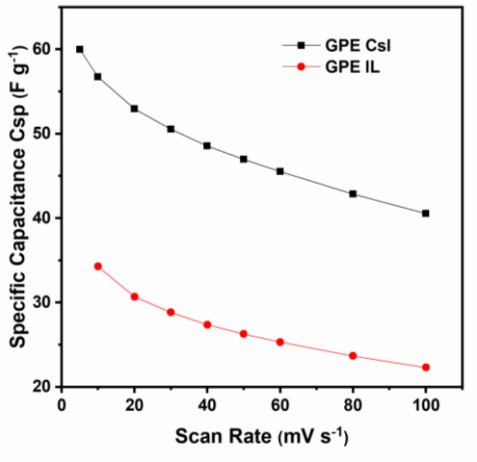


Fig 5.13. Specific Capacitance of GPE IL and GPE CsI 40 from CV curves.

Galvanostatic Charge Discharge (GCD):

The galvanostatic charge-discharge (GCD) analysis was conducted within the operating voltage range of 0 to 2V, with different current densities ranging from 0.5 to 8 A g^{-1}. Figures 6a and 6b illustrate the GCD curves of cells for varying current densities. Figure 6c showcases the GCD curves of different cells at a fixed current density of 1.5 Ag^{-1}. The triangular shape of the GCD pattern for GPE IL confirms the formation of an electrostatic (non-Faradaic) double layer between the carbon electrode and the GPE, attributed to the electrostatic interaction between the electronegative carbon electrode and the mobile ions of the GPE. The porous structure of the activated carbon (AC) influences this electrode-electrolyte interaction, with the high specific area of carbon enhancing the charge storage capacity. It is noted that the charging and discharging times decrease with an increase in the current density.

However, the GCD patterns of GPE CsI exhibit a nonlinear nature in the charging and discharging curves. This nonlinear behaviour indicates a significant pseudocapacitive contribution due to redox reactions in the cells. The presence of redox additives in the redox-active GPE increases the values of

charging/discharging time, with Cell GPE CsI 40mg showing the maximum discharge time. The specific capacitance (Csp) of the nonlinear GCD pattern were calculated using the following relations:

$$C_{sp} = \frac{4i \int V dt}{m \times (V_f^2 - V_i^2)}$$

Where i is the constant current density, $\int V dt$ is the area of discharge GCD pattern, m is the mass of the active material of a single electrode, and V_i and V_f are the initial and final voltages. The Ohmic drop is the sudden voltage drop during the discharge cycle, arising from the contact resistance between the electrode and the electrolyte interface. This voltage drop

increases with the increasing number of charging-discharging cycles of the cells. Figure 6d illustrates the variation of the specific capacitance (Csp) of different cells at different current densities.

Cell GPE CsI exhibits the highest specific capacitance of 127.93 Fg^{-1} at a current density of 1.5 A g^{-1} due to the presence of dual redox-active polymer electrolyte. This enhancement in specific capacitance, reaching more than the value of specific capacitance of GPE IL which is 88.56 F g^{-1}, is attributed to the improvement in the ionic conductivity of the dual redox-active GPE. The enhancement of specific capacitance (Csp) also influences the specific energy (Esp) and power density of the SC cell. The specific energy density and power density are given by:

$$E_{sp} = \frac{i \times \int V dt}{2 \times m}$$

The effective power density (P_{eff}) is given by:

$$P_{eff} = \frac{E_{sp}}{t_{dis}}$$

Where t_{dis} is the discharge time of the nonlinear GCD pattern. It's observed that the specific energy density of Cell GPE IL is 37.82 Wh/Kg where as that of Cell GPE CsI is 127.92 which is almost 3.4 times more at a constant current density of 1.5 A/g.

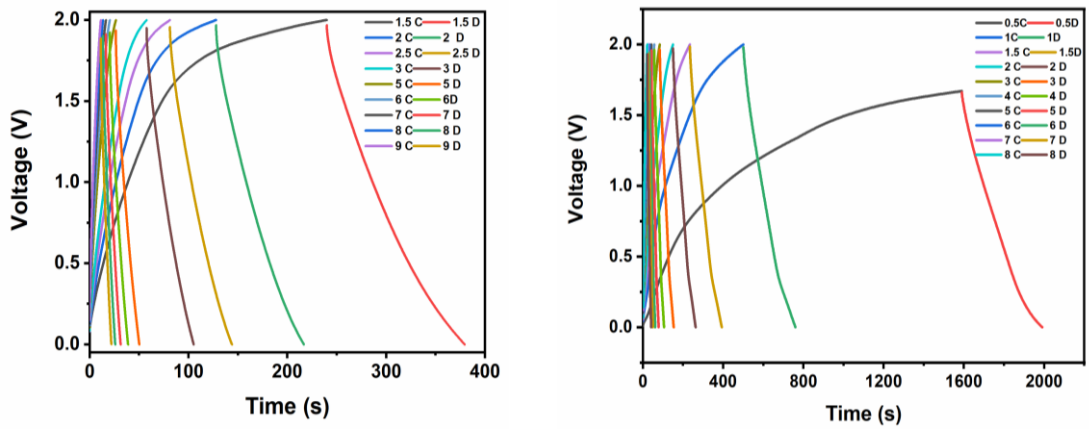


Fig.5.14. (L-R) GCD curves for (a) GPE IL and (b) GPE CsI

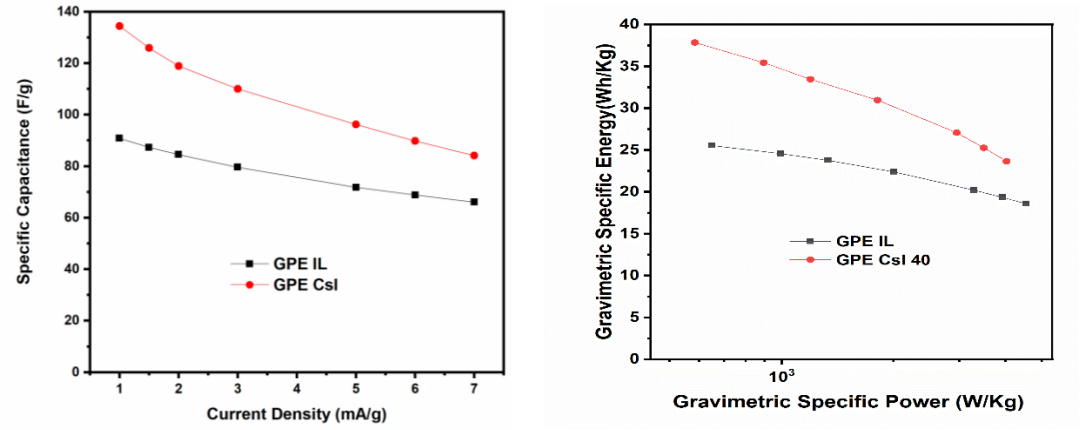


Fig. 5.15.(a) Specific Capacitance from GCD Plot **(b)** Ragone Plot for GPE IL and GPE CsI

In Fig. 5.15 we have the Ragone Plot for that confirms the formation of supercapacitor. The specific Energy is comparable with that of conventional batteries.The measurement of Coulombic Efficiency was done for over 3000 cycles at a current density of 1.5 A/g in a voltage range of 0-2 V. This initial capacitance decay could be attributed to several factors. Firstly, it may result from the blockade of small-size pores in the activated carbon (AC) electrode during the initial ion insertion and disinsertion processes of charge and discharge. Secondly, the

consumption of charge due to potential irreversible reactions of ions and redox elements absorbed on the AC electrode's surface might contribute, thus blocking pore regions and ion diffusion paths. Thirdly, an increase in interfacial resistance due to electrode degradation and electrolyte decomposition could occur. Lastly, the effective pore area might decrease due to the absorption of various byproducts during the initial galvanostatic charge-discharge (GCD) cycles.

However, despite these initial challenges, the specific capacitance stabilized after a few cycles, indicating reversible charge-discharge behaviour. Interestingly, the initial fading of all cells appeared to be nearly identical. The Coulombic efficiency of the cells was calculated using the formula: Coulombic efficiency (%) = (t_{charge} / $t_{discharge}$) × 100%, where t_{charge} and $t_{discharge}$ represent the charging and discharging times, respectively, within the specified potential range of GCD studies.

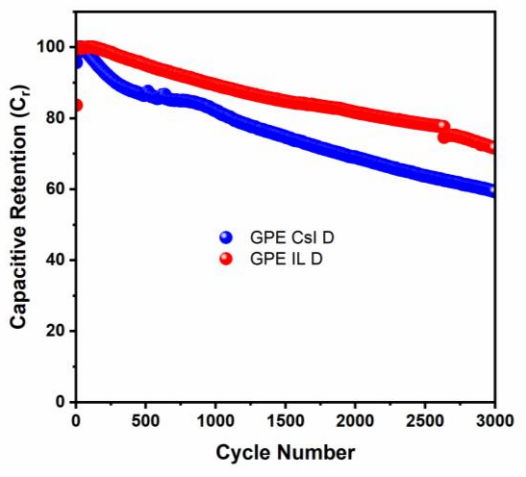


Fig.5.16. Cyclic Stability for GPE IL and GPE CsI for 3000 cycles

The Coulombic Efficiency exhibits a good stability factor for the fabricated supercapacitors. From the Long Cycle Data in Fig.5.16 we can infer that CsI sharply drops due to redox behaviour.

Electrochemical Impedance Spectroscopy (EIS):

The Electrochemical Impedance Spectroscopy (EIS) study was conducted across the frequency spectrum ranging from 10 mHz to 1 MHz, yielding insights into both bulk and interfacial properties of the SC cells. The impedance plots depicted in Figures 8a-c exhibit distinct features: a sharp rise in tails at low frequencies, indicative of capacitive behaviour, and semicircular impedance curves at higher frequencies, revealing interfacial charge transfer resistance. This resistance is primarily developed at the interface between the electrolyte and electrode surface,

while the sharp rise in impedance at low frequencies is attributed to ion diffusion through the electrode.

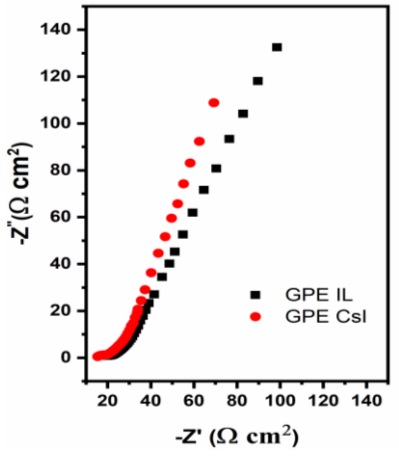


Fig.5.17. Electrochemical Impedance Plots of Cell GPE IL and Cell GPE CsI

Notably, the presence of charge transfer resistance (Rct) was not observed in double-layer carbon SC cells. However, this study reveals the presence of Rct, likely due to pseudocapacitive redox reactions occurring in Graphene-Plastic Electrolytes (GPEs) and the adsorption of various surface functionalities onto the electrode surface, such as hydroxyl (OH) and carboxyl (COOH) groups.

The specific capacitance of the SCs was determined using EIS data at a frequency of 10 mHz, employing the formula: $C_{sp} = \frac{-2}{2\pi f \times Z'' \times m}$, where Z" represents the imaginary part of impedance and m is the mass of active material in a single electrode. Interestingly, the specific capacitance calculated from the EIS study indicates that Cell GPE CsI offers greater value for the capacitance than Cell GPE CsI 40, attributed to the enhanced redox contribution in the GPE. This finding aligns well with the results obtained from cyclic voltammetry (CV) and galvanostatic charge-discharge (GCD) studies discussed earlier.

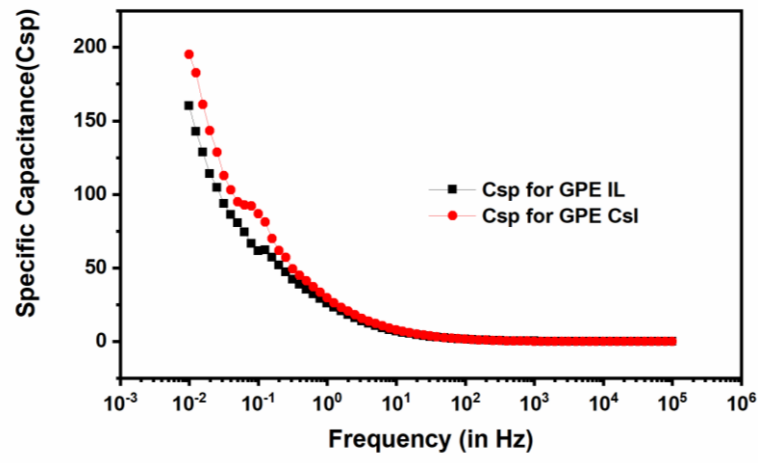


Fig.5.18. Specific Capacitance of Cell GPE IL and Cell GPE CsI from EIS plots

From the Bode Plot in Fig. 5.19. we can determine the response time of the prepared EDLC and we can find that the response time of the system has reduced significantly after addition of redox additive.

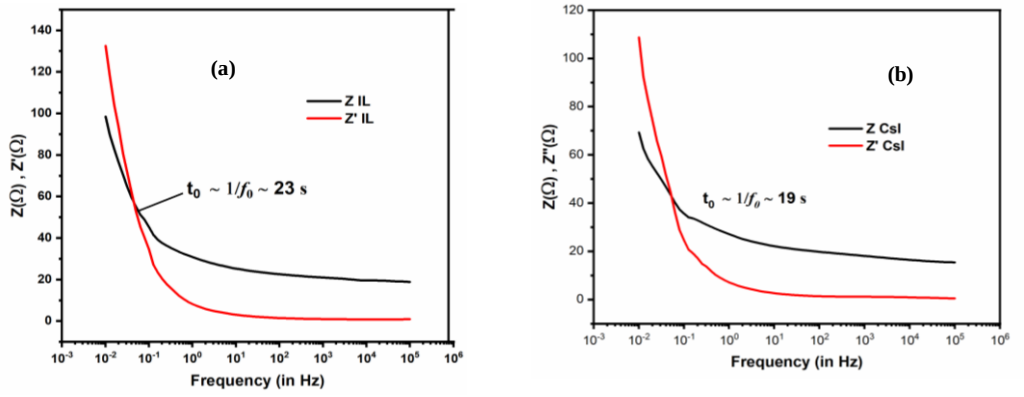


Fig.5.19. Bode Plots of Cell (a) GPE IL and (b) Cell GPE CsI

Bibliography:

(1)Ivanishchev, A. V.; Lee,S.-H.; Kim,J.-J.; Ivanishcheva, I. A.; Nam, S.-C.; Song, J.-H. Li-ion diffusion characteristics of surface modified Ni rich NCM cathode material. J. Electroanal. Chem. 2023, 932, 117242.

(2) Ivanishchev, A. V.; Bobrikov, I. A.; Ivanishcheva, I. A.; Ivanshina, O. Y. Study of structural and electrochemical characteristics of LiNi0.33Mn0.33Co0.33O2 electrode at lithium content variation. J. Electroanal. Chem. 2018, 821, 140−151.

(3)Ivanishchev, A. V.;Gridina,N. A.;Rybakov,K.S.;Ivanishcheva,I. A.; Dixit, A. Structural and electrochemical investigation of lithium ions insertion processes in polyanionic compounds of lithium and transition metals. J. Electroanal. Chem. 2020, 860, 113894. (64) Park, J.; Kim, B.; Yoo, Y.-E.; Chung, H.; Kim

(4) Zhang, J.; Jiang, J.; Li, H.; Zhao, X. A high-performance asymmetric supercapacitor fabricated with graphene-based electrodes. Energy Environ. Sci. 2011, 4 (10), 4009−4015.

(5) Ghamouss, F.; Brugere, A.; Jacquemin, J. Physicochemical Investigation of Adiponitrile-Based Electrolytes for Electrical Double Layer Capacitor. J. Phys. Chem. C 2014, 118 (26), 14107−14123.

(6) Pameté, E.; Köps, L.; Kreth, F. A.; Pohlmann, S.; Varzi, A.; Brousse, T.; Balducci, A.; Presser, V. The Many Deaths of Super capacitors: Degradation, Aging, and Performance Fading. Adv. Energy Mater. 2023, 13 (29), 2301008.

(7) Ivanishcheva, I. A.; Ivanishchev, A. V.; Chang, J. H.; Song, J.-H.; Lee, S.-H.; Kim, J.-J.; Kim, Y. J.; Nam, S.-C. Illustration of Capacity Fading Factors on the Example of La2(Li0.5Ni0.5)O4-Modified High Nickel Layered Oxide Material. Batteries Supercaps 2023, 6 (3), No. e202200466.

(8) Yadav, N.; Singh, M. K.; Yadav, N.; Hashmi, S. A. High performance quasi-solid-state supercapacitors with peanut-shell derived porous carbon. J. Power Sources 2018, 402, 133−146.

(9) cFan, L.-Q.; Zhong, J.; Wu, J.-H.; Lin, J.-M.; Huang, Y.-F. Improving the energy density of quasi-solid-state electric double-layer capacitors by introducing redox additives into gel polymer electrolytes. J. Mater. Chem. A 2014, 2 (24), 9011−9014.

Chapter 6:

Conclusion and Scope of Future Work

Cyclic Voltammetry:

The passage describes a comparative study of the electrochemical performance of two supercapacitor cells: Cell-1, which contains a gel polymer electrolyte (GPE) without CsI (potassium iodide), and Cell-2, which contains a redox-active GPE (R-GPE) with CsI.

In Cell-1, the absence of CsI results in nearly rectangular cyclic voltammetry (CV) patterns. These patterns indicate the adsorption/desorption of electrolyte ions, suggesting the formation of an electrochemical double layer at the interfaces between the electrode and electrolyte.

Conversely, Cell-2, which includes CsI in the R-GPE, displays reversible oxidation/reduction peaks at approximately +0.11 V and -0.16 V. These peaks correspond to the redox activity of iodide ions, which are ionized from the CsI, occurring at the porous activated carbon (AC) electrode/R-GPE interfaces. The reversible reactions involved are:

1. $3I^- - 2e^- \leftrightarrow I_3^-$

2. $2I^- - 2e^- \leftrightarrow I_2$

3. $2I_3 - 2e^- \leftrightarrow 3I_2$

These reactions demonstrate the redox activity of iodide ions, which contribute to the electrochemical performance enhancement observed in Cell-2.

Galvanostatic Charge Discharge:

The high capacitance values observed in capacitor cells utilizing redox-active electrolytes depend on the suitable combination of the shape/size of redox species/ions (such as I^-, I^{3-}, and I^{5-} in this case) and favorable pore sizes in the carbon electrodes. In the present context, iodide ions (I^-), when combined with I_2 molecules, form redox species like I^{3-}, I^{5-}, etc., during electrochemical reactions at the interfacial region.

Iodide ion (I^-) has a spherical shape with a size of 0.39 nm, while I3^- and I5^- ions are ellipsoids with sizes of 0.63 nm and 1.8 **nm**, and 1.2 **nm** and 1.26 **nm**, respectively. The presence of smaller redox ions (I^-, I^{3-}-, I^{5-}, etc.) in the polymer matrix of R-GPE allows for more active sites for redox ions at the electrode/electrolyte interface due to the availability of smaller porosity in carbon electrodes, such as micropores (≤ 2 nm) and mesopores (≥2 nm), as found in the

PAC and CAC electrodes.

This enables a larger amount of insertion/de-insertion of redox species into the porous interiors of AC electrodes, facilitating fast pseudo-capacitive reactions. Consequently, improving its parameters such as capacitance, energy, and power.

Initial capacitance fading in porous activated carbon can be attributed to two main factors. Firstly, the diverse surface functionalities present in activated carbon tend to undergo surface reactions with electrolyte ions like $BMIM^{+}$, $TFSI^{-}$, Cs^{+}, and I^{-}. These reactions lead to irreversible charge consumption, resulting in the observed initial capacitance fading. The existence of various functional groups such as OH and COOH on the surface of porous carbon has been confirmed through FTIR analysis. Secondly, another cause of initial capacitance fading is the blockage of micro-pores in the carbon electrodes during the initial adsorption and desorption of electrolyte ions. This blockage renders these pores inaccessible to electrolyte ions after the initial few cycles, contributing to the reduction in capacitance.

Electrochemical Impedance Spectroscopy (EIS):

In both cell configurations, featuring GPEs with and without the redox CsI additive, a pronounced capacitive behavior is observed in the low-frequency region, extending up to 10 mHz. Notably, distinct differences in the EIS (Electrochemical Impedance Spectroscopy) patterns are evident, particularly in the mid-frequency range, highlighting the influence of the electrolyte composition, particularly the role of the redox-additive CsI.

In Cell-1, utilizing GPE without CsI, a sharp increase in EIS pattern occurs immediately after a semicircular spur in the mid-frequency range, indicating the formation of a proper capacitive double layer at the interface. Conversely, in Cell-2 (with Redox active GPE), a slightly curved nature of EIS variation is observed in the mid-frequency region. Such curvature in the EIS pattern in the mid-frequency region for cells with CsI-containing GPEs is attributed to the redox activities at the electrode/electrolyte interfaces due to iodide ions.

This mid-frequency behavior is succeeded by a steep rise pattern in the lower

frequency region, attributed to the capacitive nature of the device arising from the formation of a double layer by electrolyte ions (BMIM+, TFSI-, and K+).

Conclusion:

A non-aqueous redox-active GPE film, incorporating an IL (EMITFSI) with the addition of redox-additive CsI, embedded within a PVdF-HFP polymer matrix, has been developed and optimized for application as a quasi-solid electrolyte in carbon supercapacitors. Comprehensive thermal, and electrochemical analyses affirm the suitability of these RGPE films for supercapacitor use, exhibiting flexibility and thermal stability (up to approximately 250°C), high room temperature ionic conductivity (around 3.9 × 10^3 S cm^-1), and wide electrochemical stability window (ESW) of approximately 5.75 V.

Symmetrical quasi-solid supercapacitors have been fabricated utilizing AC-electrodes paired with RGPE films containing CsI. Comparative studies have been conducted with GPE (without KI) through EIS, CV, and GCD tests over numerous charge-discharge cycles. The incorporation of CsI in the GPE leads to strong cathodic and anodic peaks in CV and plateaus in GCD curves, indicating redox activity at the interfaces of AC-electrodes and R-GPE based cells. Consequently, GPE-CsI 40 based supercapacitor cells exhibit larger specific capacitance (135 F/g), higher specific energy (37.8 Wh/kg), and high specific power value compared to cells with GPE without CsI (C_{sp} 90.8 F/g,E_{sp} 25.53Wh/kg).

The capacitor cells incorporating the redox additive CsI demonstrate favorable rate performance as observed from EIS, CV, and GCD measurements. Additionally, these redox-active capacitor cells exhibit robust cycling performance up to approximately 3000 cycles with only around 11% initial capacitance fading and 75–90% Coulombic efficiency.

In today’s context, the escalating demand for energy coupled with the diminishing reservoirs of fossil fuels underscores the urgent need for the development of energy

storage solutions that are high-performing, cost-effective, environmentally friendly, and sustainable. Among the array of options available, electrochemical capacitors, commonly known as supercapacitors, have garnered considerable attention over the past few decades. This is owing to their superior energy density compared to traditional capacitors, impressive power density relative to batteries, and extended cycling life.

Researchers worldwide are actively engaged in endeavors aimed at boosting the energy density of supercapacitors while preserving their power density. Key parameters influencing the energy density of these devices include the specific surface area and porosity of the electrodes, along with the electrochemical properties of the electrolytes, such as their stability window and ionic conductivity. Additionally, the integration of rapid redox activity at the interfaces by incorporating redox-additives into electrolytes represents a pivotal strategy for augmenting the energy density of supercapacitors. This inclusion facilitates an additional pseudo-capacitive contribution, thereby enhancing overall performance.

While numerous studies in the literature have explored this approach using aqueous electrolyte systems, only a limited number of reports exist on capacitors employing non-aqueous redox-active polymer-based electrolytes. These systems not only boast high ionic conductivity but also offer a broad electrochemical stability window, making them promising candidates for advancing the capabilities of energy storage devices.

Scope of Future Work:

- We can conduct free volume test and PAL's (Positron Annihilation Analysis) to understand AC conductivity.
- Dual redox based supercapacitor can be fabricated to enhance electrochemical parameters such as specific capacitance Power and Energy
- In Li^+ ion battery redox additive increases interfacial stability and enhances the Lithium-ion transport number by making it dendrite free.
- We could also use activated carbon from bio-degradable source instead of commercial Activated Carbon (CAC) to increase porosity.

Bibliography:

[1] P. Simon, T. Brousse, F. Favier, Supercapacitors Based on Carbon or Pseudocapacitive Materials, ISTE Limited (2017).

[2] F. Beguin, E. Frackowiak, Carbons for Electrochemical Energy Storage and Conversion Systems, CRC Press, 2009.

[3] M. Lu, Supercapacitors: Materials, Systems, and Applications, John Wiley & Sons, 2013.

[4] A. Yu, V. Chabot, J. Zhang, Electrochemical Supercapacitors for Energy Storage and Delivery: Fundamentals and Applications, Taylor & Francis, 2013.

[5] T. Li, R. Ma, J. Lin, Y. Hu, P. Zhang, S. Sun, L. Fang, The synthesis and performance analysis of various biomass-based carbon materials for electric double-layer capacitors: a review, Int. J. Energy Res. 44 (2020) 2426–2454, https://doi.org/10.1002/er.5061.

[6] N. Kularatna, K. Gunawardane, Energy Storage Devices For Electronic Systems: Rechargeable Batteries and Supercapacitors, Academic Press, 2021.

[7] A.K. S.hukla, S. Sampath, K. Vijayamohanan, Electrochemical supercapacitors: energy storage beyond batteries, Current Sci 79 (2000) 1656–1661. https://www.jstor.org/stable/24104124.

[8] J. Zhong, L.Q. Fan, X. Wu, J.H. Wu, G.J. Liu, J.M. Lin, M...L. Huang, Y.L. Wei, Improved energy density of quasi-solid-state supercapacitors using sandwich-type redox-active gel polymer electrolytes, Electrochim. Acta 166 (2015) 150–156, https://doi.org/10.1016/j.electacta.2015.03.114.

[9] C. Zhong, Y. Deng, W. Hu, D. Sun, X. Han, J. Qiao, J. Zhang, Electrolytes for Electrochemical Supercapacitors, CRC press, 2016.

[10] C. Zhong, Y. Deng, W. Hu, J. Qiao, L. Zhang, J. Zhang, A review of electrolyte materials and compositions for electrochemical supercapacitors, Chem. Soc. Rev. 44 (2015) 7484–7539, https://doi.org/10.1039/C5CS00303B.

[11] M.A. S.cibioh, V. Balasubramanian, Materials for Supercapacitor Applications, Elsevier, 2020. [12] C. Zhao, W. Zheng, A review for aqueous electrochemical supercapacitors, Front. Energy Res. 3 (2015) 23, https://doi.org/10.3389/fenrg.2015.00023.

[13] S.A. Hashmi, N. Yadav, M.K. Singh, Polymer electrolytes for supercapacitor and challenges, in: T. Winie, A.K. Arof, S. Thomas (Eds.), Polymer Electrolytes, Characterization Techniques and Energy Applications, Wiley-VCH, 2019, pp. 231–297.

[14] X. Cheng, J. Pan, Y. Zhao, M. Liao, H. Peng, Gel polymer electrolytes for electrochemical energy storage, Adv. Energy Mater. 8 (2018), 1702184, https:// doi.org/10.1002/aenm.201702184.

[15] S.A. Hashmi, Supercapacitor: an emerging power source, Natl. Acad. Sci. Lett. 27 (2004) 27–46.

[16] Q.M. Tu, L.Q. Fan, F. Pan, J.L. Huang, Y. Gu, J.M. Lin, M.L. Huang, Y.F. Huang, J. H. Wu, Design of a novel redox-active gel polymer electrolyte with a dual-role ionic liquid for flexible supercapacitors, Electrochim. Acta 268 (2018) 562–568, https:// doi.org/10.1016/j.electacta.2018.02.008.

[17] G.P. Pandey, T. Liu, C. Hancock, Y. Li, X.S. Sun, J. Li, Thermostable gel polymer electrolyte based on succinonitrile and ionic liquid for high-performance solid-state supercapacitors, J. Power Sources 328 (2016) 510–519, https://doi.org/10.1016/j. jpowsour.2016.08.032.

[18] G.P. Pandey, S.A. Hashmi, Experimental investigations of an ionic-liquid-based, magnesium ion conducting, polymer gel electrolyte, J. Power Sources 187 (20